

Date of Report: <November 15, 2015>

Contract Number: <DTPH56-13-H-CAAP05>

Prepared for: <Government Agency: U. S. DOT PHMSA >

Project Title: <Composite Self-Sensing Thermal Sprayed Coatings for Pipeline Corrosion Prevention and Mitigation>

Prepared by: <North Dakota State University>

Contact Information: <Dr. Fardad Azarmi, Email: fardad.azarmi@ndsu.edu, Phone: 701.231.9784; Dr. Ying Huang, Email: ying.huang@ndsu.edu, Phone: 701.231.7651.>

For CAAP Draft Final Report period ending: <November 15, 2015>

Business and Activity Section

(a) Generated Commitments

No changes to the existing agreement.

No equipment purchased over this reporting period.

Materials purchased over this reporting period:

Self-centering jaw, Hot rolled pipes, Copper fittings, Tubing, Couplings, Drill bits, OS1100 FBG Sensors. Copper powder for spraying, and extra hard drive for data storage.

(b) Draft Final Report

1 Introduction

1.1 Different Types of Corrosion on Buried Pipeline

Common causes of corrosion on underground pipelines include low-resistivity soils, anaerobic bacteria, dissimilar metals, differences in soil composition, differential aeration of the soil around the pipe, and stray direct current from external sources. These factors follow by different types of corrosion on the pipeline the most important and common of which are pitting, selective seam corrosion, microbial corrosion, stray current corrosion, and galvanic corrosion. These types of corrosion will be illustrated briefly in the following.

1.1.2 Pitting

It has been reported that the most common type of corrosion on pipelines is pitting rather than uniform reduction of the wall thickness^{1,2}. The reason would be due to the fact that during the corrosion the environment of anodic area tends to become more acidic. In fact, the iron ions in solution react with the hydroxyl ions of the water to generate an excess of hydrogen ion which makes the anodic environment more acidic which tends to localized corrosion^{1,2}.



On the other hand, hydroxyl ions produced at the cathodic area makes it less acidic and less likely to get corroded. In conclusion, by creating a pit on the surface, consecutive corrosive attack tends to concentrated at that location. Therefore, pitting is most likely to occur on the surface rather than the uniform reduction in wall thickness. However, the pits may overlap and produce a general but irregular thinning of the pipe wall.

1.1.3 Selective Seam Corrosion

Most of the pipe installed in the industry are seamed or welded. Two typical welding methods have been used for this aim are submerged-arc welding or upset-butt welding. The filler used for submerged-arc welding contains compositions slightly different from that of the body of the pipe. Furthermore, both welding methods provide heat affected zone next to the weld metal which have different microstructure than the rest of the pipe due to the dissimilar cooling rates of different parts of this zone during the welding process. The seam itself also might contain of cracks, flaws, or discontinuities. These factors make the pipe more susceptible to corrosion ^{1, 2}.

1.1.4 Microbial Corrosion

Microbiologically Influenced Corrosion (MIC) is generally caused by bacteria, moulds, and fungi or their by-products which results in degradation of materials. There are two possible acts ³.

- Acid by-products, such as Sulphur, hydrogen sulphide or ammonia attack the pipe or the protective layer. The main types are sulfate-reducing bacteria (SRB) and acid-producing bacteria (APB).
- Direct interaction between the microbes and the metal which are in contact with each other.

1.1.5 Stray Current Corrosion

Stray current corrosion usually occurs when a direct current flows through unintended path and the flow of electrons supports corrosion. This phenomenon can occur in soils and flowing or stationary fluids. There are several common methods to control the current and reduce the corresponding corrosion. Insulation, using earthing sources, cathodic protection, and sacrificial anode are the most common methods to mitigate and inhibit the stray current corrosion ^{4, 5}.

1.1.6 Galvanic Corrosion

When two different metals with different electronegativities are placed in contact with each other galvanic corrosion occurs. In this case the metal with higher willingness of giving up electron will act as an anode and the one with the higher electronegativity will attract electron and create an electrochemical cell and corrosion will take place. However, there are some special features and prerequisites for the galvanic corrosion to occur. First, the metals should be electrically in contact. Next, the difference in electronegativity of the two metals should be such that one metal be significantly better at giving up electrons than the other. Last but not least, an additional path for ion and electron movement is necessary (suitable electrolyte). Using a proper insulator or coating to avoid the electrical contact between the metals is a common method to prohibit the galvanic corrosion. Another solution would be selection of metals close to each other in galvanic series ¹.

1.1.7 Mechanism of Corrosion in Onshore Pipeline

In scientific stand point, corrosion has been well understood both in terms of casual mechanism and also methods of control. However, it has been reported that pipelines, either buried or on the ground, continue to experience a modest but notable number of failure attributed to corrosion. In fact corrosion behavior of a buried pipeline is a way more sophisticated than that of a piece of steel in a beaker of salt water. There are several features that make this behavior more complicated for the buried pipeline ¹:

- The chemical properties of the surrounding environment of a buried pipeline are not understood adequately.
- The oxygen content, moisture content, chemical composition of the soil along pipe length and from top to bottom of the pipe can act as concentration cells that promote corrosion.
- Moisture and oxygen content in the soil also varies with time.
- The quality of the coating also is not exactly equal along the pipe.
- Coating sometimes becomes disbanded from the pipe surface, allowing groundwater to contact the steel but shielding the steel from cathodic-protection current.

- Disbanded coating will prevent aboveground survey detection of underlying corrosive conditions.
- Physical variations in soil characteristics and placement (gaps, etc.) affect the distribution of cathodic-protection current.
- Visual inspection of the outside of the pipe and the coating require excavation.
- Stray current from nearby buried structures can interfere with a pipeline's cathodic-protection system.

Taking all the above factors in to the consideration, preventing corrosion in a very large size metal structure would face challenging problems. Thus, it is valuable to design a method to reduce the interfering of these factors to monitor and assess the corrosion in the pipeline more accurately.

1.2 Corrosion Mitigation

Corrosion prevention and mitigation has been long recognized as a critical task for pipeline industry. Two major methods were widely deployed for pipeline corrosion prevention including cathodic protection and coating techniques ⁶.

1.2.1 Cathodic Protection

Cathodic environments, which significantly accelerate the pipeline corrosion and introduce pin-point corrosions on pipelines, are needed to be prevented. Cathodic protection, therefore, makes its way for protection of most of the metal pipeline ². Sacrificial anode ⁷ and impressed current anode ⁸ are two commonly used cathodic protection methods. For sacrificial anode, an electronegative metal such as Zinc or Magnesium is connected externally to the pipeline, inducing the corrosion mass loss of the sacrificial metal instead of metal pipeline. On the other hand, impressed current anode method applies direct current between the anode and the pipeline to prevent the occurrence of cathodic environments. Individual cathodic protection limits the corrosion resistances and requires extremely high external current, demanding other technologies for corrosion prevention such as the development of coating techniques.

1.2.2 Coating Techniques

Non-metallic coatings separate the metal pipeline from the surrounding corrosive environments, showing a good performance on corrosion mitigation. Coal tar coatings ⁹ were designed and applied to pipeline before 1970s, which were difficult to apply and environmentally unfriendly. For a safer, faster, stronger, and easier coating, solid rigid polyurethane coating ¹⁰ were developed for pipeline corrosion prevention in 1970s and replaced the coal tar based coating in 1980s. Since thin solid rigid polyurethane coatings may fail corrosion protection after long-term uses, thick layered coatings were developed in 1990s including polychloroprene coating ¹¹, Fusion-Bonded Epoxy-(FBE) coating ¹² and 3-Layer-Polyurethane coating (3LPE) ¹³. Combined with concrete, the FBE or 3LPE coatings were widely deployed in off-shore pipelines. However, these thick polymer coatings have the disadvantages such as high cost and high potential for initial defects.

Metallic coatings using thermal spraying techniques had also been researched for pipeline corrosion protection ^{14, 16}. Thermal Spraying Process is a general name for a group of deposition processes in which solid particles are melted and accelerated toward a substrate. The different methods of thermal spraying are classified based on the energy sources which are chemical and electrical ¹⁷. Conventional Flame Spray and High Velocity Oxygen Fuel (HVOF) are among the techniques which rely on chemical energy as to melt the particles while Air Plasma Spraying (APS) and Wire Arc Spraying are examples of methods which are solely based on electrical energy. Some techniques such as HVOF and APS have been broadly used and commercialized by several industries during the recent decades ¹⁸. Industries such as aerospace, automotive, bioengineering, marine, and civil structures are among the ones which adopted thermal spraying as a method for coating into their system ¹⁹⁻²⁴. Thermal spray processes can also be used as a method to repair damaged surfaces of industrial components ²⁰. The capability of applying a variety of coatings on to the different substrates has made thermal spraying an attractive industrial tool to protect, repair and manufacture of advanced structures and materials.

Gaining interests on thermal spraying of metallic coatings were expanded to the off-shore pipelines ^{15, 16} and successfully applied to water related structures such as Mormon Flat dam ^{21, 22}. The thermally sprayed metallic

coatings can act both as cathodic protection and speration layer. The cathodic measures of these metallic coating drastically reduced the dependence on external supplemental anodes. These coatings has been shown as a cost-effective corrosion protection way which significantly enhances corrosion mitigation in a wide range of tempeature environments. The performance of coating can be defined by controlling composition, and the selection of deposition technique. Generally, the thermally sprayed coating has shown better protection and longevity compared to the other traditional coating technology. A wide variety of ceraqmics, metals, and metallic alloys can be deposited using thermal spraying technique.

1.3 Sensing Technology for Corrosion Assessments

To assess corrosion, currently, the well-investigated techniques have been primarily based on qualitative visual inspections with nondestructive evaluation tools. Existing technologies can be divided into several different categories including electrochemical, physical, and material sacrificial methods.

1.3.1 Electrochemical Approach

An electrochemical approach is widely applied for direct corrosion assessment tool which helps to understand the corrosion mechanism. The electrochemical method measures the average corrosion effects by quantifying the electrical fields/potentials at the steel surface or measuring the corrosion environmental factors such as chloride content and pH of pore fluids ^{25, 26}.

Corrosion normally occurs at a rate determined by an equilibrium between opposing electrochemical reactions. One is the anodic reaction which releases elections into metal and is oxidized. Another one is cathodic reaction which absorbs electrons from metal. Since these two reactions are in state of equilibrium, or the net flow of electrons from each reaction is zero, no electrical current flow occurs. The potential of the metal could be measured by the state of equilibrium of anodic and cathodic reactions. The equilibrium potential estimated by the metal in the absence of electrical connections to the metal is called open circuit potential. It is the primary data should be detected in most of electrochemical corrosion test.

A stable Open Circuit Potential, reflects as a steady state of electrons exchange, is critical number before starting the electrochemical test. Under the steady state, the corrosion reaction rate could be assumed as constant. The value of either the anodic or cathodic currents at open circuit potential generally is known as corrosion current. The corrosion current is not measureable directly. Instead, the estimation of current versus potential curve could be a good solution to get the corrosion current indirectly since the voltage will be centered on open circuit potential. This procedure is called Tafel test, the equation for single isolated reaction is Tafel equation ^{27, 28}:

$$I = I_0 e^{(2.3(E-E^{\circ})/\beta)} \quad (2)$$

where the I_0 is exchange current, E is the electrode potential, E° is the equilibrium potential, and β is the reaction's Tafel constant with unit volts/decade.

The equation could describe both the anodic and cathodic reaction is called Butler-Volmer equation ²⁸:

$$I = I_a + I_c = I_{corr} (e^{(2.3(E-E_{oc})/\beta_a)} - e^{(-2.3(E-E_{oc})/\beta_c)}) \quad (3)$$

where E_{oc} is the corrosion potential in volts, β_a is the anodic Tafel constant, and β_c is cathodic Tafel constant.

Simplifying the Bulter-Volmer equation based on the idea that is by restricting the potential close to corrosion potential, the current versus voltage curve is an approximately straight line. The slope of this curve is called polarization resistance with unit of ohms. In case to calculate the corrosion current, combine the polarization resistance with the Tafel constant could be summarized as the Stern-Geary equation ²⁸:

$$I_{corr} = \frac{\beta_a \beta_c}{2.3R_p (\beta_a + \beta_c)} \quad (4)$$

where the R_p is the polarization resistance in ohms.

Based on the Faraday's Law, then use the conversion of weight loss of object to corrosion rate, a modified equation to compute the corrosion rate with Faraday's law had been performed ²⁸:

$$CR = \frac{I_{corr} \cdot K \cdot EW}{d \cdot A} \quad (5)$$

In which, CR represents corrosion rate with unit mm per year or milli-inches per year, K is a constant defines corrosion rate, EW is the equivalent weight of object, d is the density of testing material, and A is the testing area. In this equation, K could be expressed as 3,272 mm/apm-cm-year if the corrosion rate unit is mm/year, or 1.288×10^5 milli-inches/apm-cm-year with corrosion rate unit is milli-inches/year.

1.3.2 The State-of-art Sensing Technology

Other than an electrochemical method, a physical approach is an indirect corrosion assessment means which monitors the corrosion-induced structural degradations through measuring various physical quantities such as strain, guided wave, ultrasonic, and acoustic waves ^{24, 25}. While the two other methods provide average corrosion assessment, the material sacrificial approach is valuable to pin-point corrosion. It directly measures the corrosion-induced loss of materials by monitoring, for example, the loss of coated metallic thin film materials ³¹⁻³³, the change in resistance/conductivity ³² and the change in embedded metal antennas ²⁹. However, to date, limited approaches could perform real-time remote corrosion monitoring for large-scale structures in a cost-effective manner.

Fiber optic sensors, with their unique advantages such as multi-parameter and quasi-distributed sensing, long-term remote monitoring in real time, and low cost ³⁵, have been expected to provide a potential cost-effective tool for real-time remote corrosion assessment of large-scale structures. Fiber optic corrosion sensors have been investigated based on material sacrificial and physical approaches. Material sacrificial based fiber optic sensors usually monitor the light intensity changes induced by the thickness changes of the metal film coatings on the cleaved end of a fiber or out surface of an uncladded fiber. These metal film coatings include Fe-C alloy, iron ²⁶, an electro less deposit of Ni-P, aluminum ^{26, 37}, nickel (magnetic field vacuum deposition), and silver (chemical sputtering plating) ³⁸. Such a coated optical fiber sensor is simple in concept, but monitors only one single point of steel structures. Multiplexing becomes a critical concern for monitoring in large scale. More importantly, the fragile nature of the uncladded fiber increases the chances for installation damage.

The physical based optical fiber corrosion sensors relies on fiber grating techniques including Fiber Bragg Grating (FBG) and Long Period Fiber Grating (LPFG) sensors. FBG sensors packaged or coated by Fiber Reinforced Polymers (FRP) ³⁴ and Fe-C alloy ^{40, 41} was developed for steel corrosion monitoring by wrapping the sensor on the steel bar to be monitored. Strain was measured to further relate to the corresponding steel corrosion. LPFG based optical fiber sensors, on the other hand, monitored the corrosion environments which can be related to the corrosion process including moisture, pH, and metal ion sensors ⁴². For each LPFG chemical based corrosion sensor, a unique target-specific coating was applied to the surface the LPFG and optimized for specificity, responsiveness, and reliability. Direct monitoring of the corrosion process based on LPFG sensors have not yet been fully explored and very few techniques are developed specifically for pipeline corrosion assesemnts.

1.4 Summary

2 Material Selection for Corrosion-Resistant Thermal Spraying Coating

2.1 Thermal Spraying Metallic Coating Materials

Various coating materials are available for thermal spraying coatings. Table 1 compares the long-term performances of various thermal spraying metallic coating materials for off-shore pipeline corrosion mitigation which performed by previous studies ^{10, 11}. It can be seen from Table 1 that Zinc (Zn), Aluminum (Al), and their alloys were the most investigated materials for thermal spray coating on pipelines. Pure Zn experienced a poor corrosion resistance with or without consideration of sealing. Pure Al was experiencing a fair performance using

acr spray and a poor performance using a flame spray technique. The increase of the Al spray coating thickness did not result in a better corrosion prevention. If combined with epoxy sealing, Arc spray Al coating performed better than flame spray Al coating in a long run. If polyurethane paint was used as sealing, flame sprayed Al coating showed the best long-term resistance. More importantly, if composite materials were applied for flame spray such as Zn-Al, Cu-Al, and Cu-P alloy, the long-term corrosion mitigation performance improved significantly with combination of the epoxy sealing technique. Thus, for on-shore metal pipelines, composite metal alloys such as Cu-Al alloy would be the best potential thermal spray metallic coating materials. In addition, epoxy and polyurethane may be good candidates for further coating sealing purpose.

Table 1 Summary of thermal spray metallic coating materials, the advantages, and disadvantages for pipeline corrosion mitigation^{11, 17}.

<i>Performance Ranking</i>	<i>Spray Metal</i>	<i>Spray Process</i>	<i>Spray Thickness (μm)</i>	<i>Sealing Material</i>	<i>Performance at Marine Environments</i>	<i>Comments</i>
1	Al	Flame	175	WP+PU	<i>Tier 1: Excellent long-term performance: Sound without change in coating</i>	<i>The material of aluminum is cost-effective, excellent corrosion resistance up to 15 years, but the PU sealing is expensive</i>
2	Zn-Al alloy	Flame	175	Epoxy		<i>87% Zn & 13% Al</i>
3	Al	Arc	175	Epoxy		<i>The material of aluminum is cost-effective, local spotty white rust in tidal environments</i>
4	Cu-Al alloy	Flame	175	Epoxy		<i>Excellent long-term performance up to 15 years, and adding some powders of Iron, Cobalt, and Nickel will further enhance the corrosion and cracking resistance</i>
5	Zn-Al alloy	Flame	175	None	<i>Tier 2: Good long-term performance: Local spotty white rust on coating surface</i>	<i>87% Zn & 13% Al</i>
6	Al	Arc	175	None		<i>Fair performance in flash zone</i>
7	Al	Arc	400	None		<i>Fair performance in flash zone and if appropriate thickness meets, thicker coating does not help</i>
8	Al	Flame	175	Epoxy	<i>Tier 3: Fair long-term performance: Change in coating color</i>	<i>Fair performance in tidal zone</i>
9	Zn	Flame	175	WP+PE+PU	<i>Tier 4: Poor long-term performance: Local coating damage and red spotty rust</i>	<i>Good short-term performance in the first 7 years but poor long-term performance after that, and the complexity of the sealing process make the coating process time consuming and expansive</i>
10	Al	Arc	400	CP+PE+PU		
11	Zn	Flame	175	Epoxy	<i>Tier 5: Very poor long-term performance: general red rust and damage of coatings</i>	<i>Poor short- and long-term corrosion resistance in the tidal zone within and after 7 years</i>
12	Zn	Flame	175	None		<i>Fair short-term performance within 7 years but very poor long-term performance in the tidal zone after then</i>
13	Al	Flame	175	None		<i>Fair short-term corrosion resistance in the splash and tidal zone within 7 years but very poor long-term behavior since then</i>

2.2 Systemical Materials Selection Using CES Software

To systemically select the materials for pipeline corrosion mitigation using thermal spraying coating technique, CES software had been used in this study. CES is a commercially available software which is widely used by material scientists for accurate material selection. The material selection using CES has been performed based on some fundamental criteria including: material durability at fresh water, alkali and acidic soil, material processability (ability to be thermal sprayed), cost, flammability, and mechanical properties such as fracture toughness.

According to the results obtained from CES software (Figure 1), several material groups were found to be effective in corrosion prevention for steel pipelines including nickel based alloys, tungsten alloys, stainless steel, zinc alloy (Zn+ 3-30% Al, typically, often with up to 3% Cu), and copper based alloys. As it can be seen from Figure 1, Nickel based alloys and Tungsten alloys are the most expensive materials for deposition by the average price of \$13.9/lb and \$10.1/lb, respectively. The Tungsten alloy's corrosion resistance in water (salt) is not significant improved compared to steel while relatively expensive, thus they can be substituted by the other alloys such as zinc and copper based alloys. Nickel-based alloys usually are used when resistance to high-temperature corrosion is required, which is not required in this study. Thus, by taking all the mentioned facts above into the consideration, copper alloys are considered to be a promising coating materials for corrosion prevention of the steel pipes.

Copper and copper alloys have been shown excellent corrosion resistance in atmospheric and aqueous environments. Historically, copper and its alloys have been used for corrosion protection in different industries. They are mostly utilized for protection against bio-fouling and crevice corrosion which are generally associated with sea water service condition. Among the various metals commonly employed for underground application (e.g., copper, iron, lead, and zinc, the latter usually as galvanized coating on steel), copper and its alloys have shown the best performance³⁶. Figure 2 shows the corrosion rate, representing as maximum penetration in millimeter, for copper, iron, lead, and zinc in four kinds of soils including (1) well aerated acid soils low in soluble salt (Cecil Clay Loam), (2) poorly aerated soils (Lake Charles Clay), (3) Alkaline soils (Docas Clay), and (4) soils high in sulfides (Rifle Peat). Copper corroded the least, and much less than the other three metals in all four types of soils^{36, 37}. Thus, in this study, copper (Cu) and copper alloys, specifically, Cu and Cu-Al Bronze Alloy, are selected to be used as thermal spraying materials for corrosion prevention of buried steel pipelines.

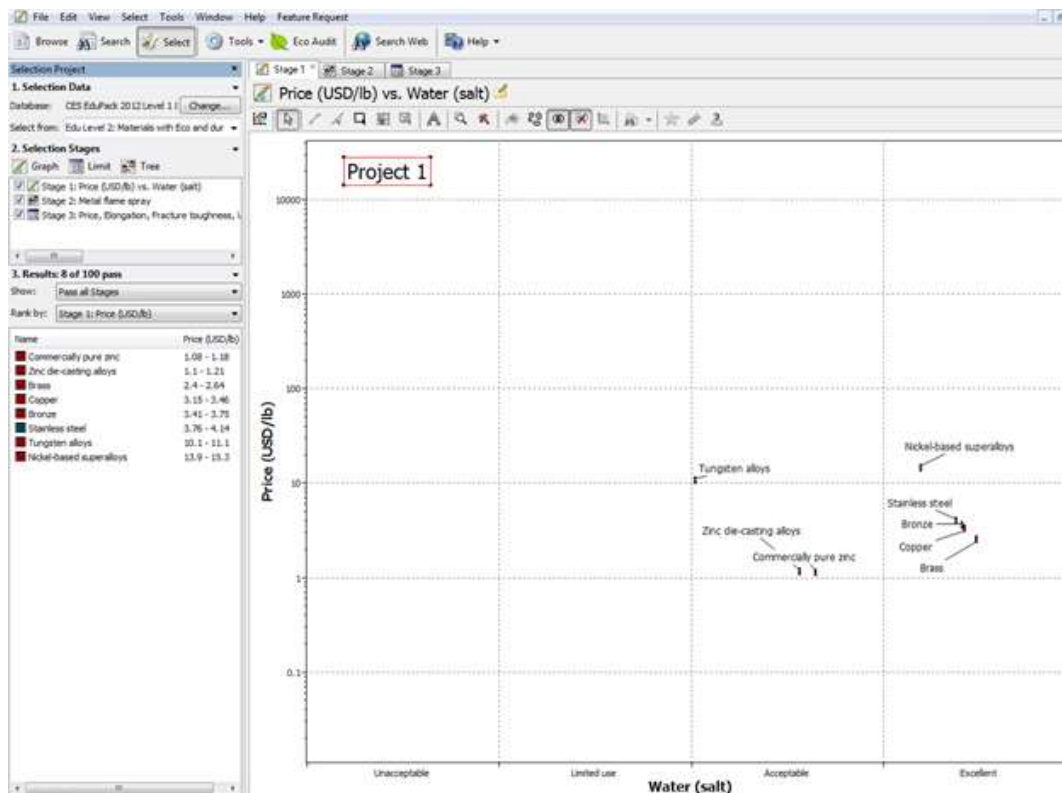


Figure 1 A screen shot from CES program as used for materials selection.

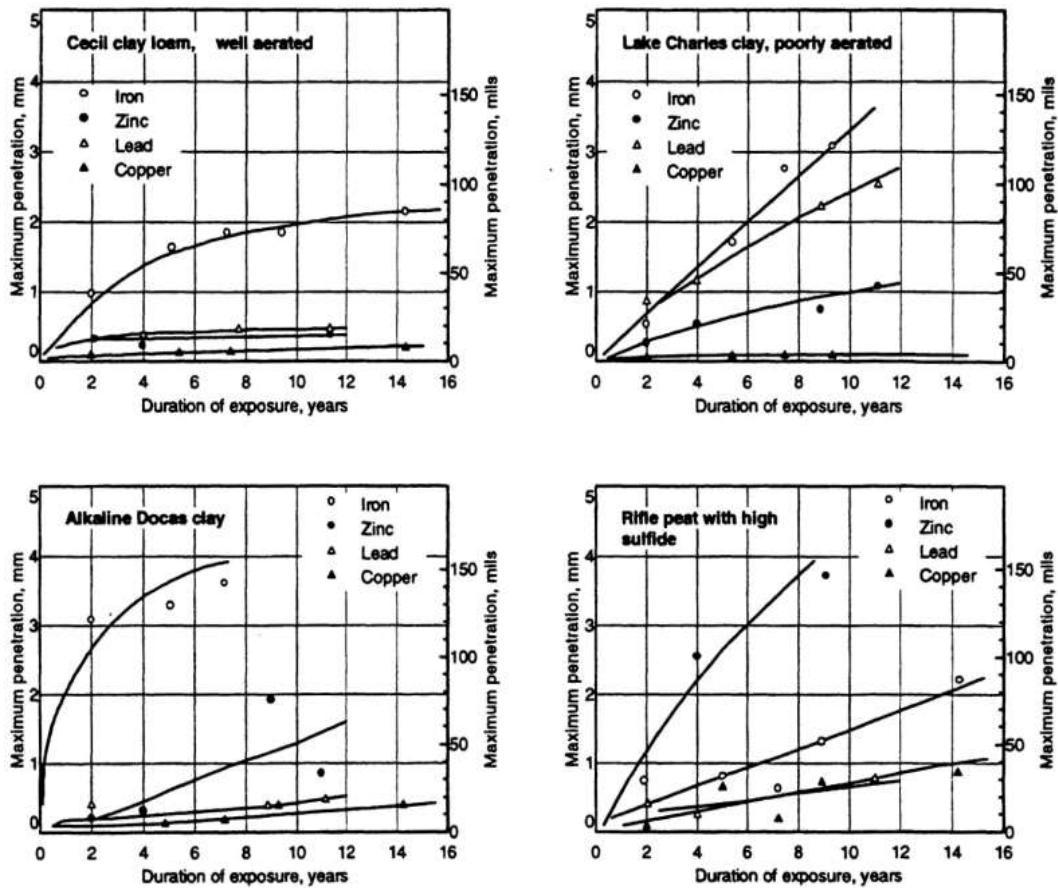


Figure 2 Corrosion of copper, iron, lead, and zinc in four different soils³⁶.

2.3 Material Characterization of Cu and Cu-Al Bronze Alloy

To investigate the capability of Cu and Cu-Al Bronze Alloy for corrosion protection as thermal spraying coating, their material properties were characterized for their microstructure, hardness, and corrosion resistance.

2.3.1 Microstructure of Cu and Cu-Al Bronze Coating

The microstructure of the thermal sprayed coating is an important factor to be considered for the material property because it can indicate the porosity of the coating. The average level of porosity which usually effects mechanical property of the coating such as elastic modulus, strength, and hardness.

Figure 3 shows the microstructure of copper coating deposited using HVOF technique. The lamellae type structure is visible and coating is uniform. The coating thickness was approximately 800 μ m. Image analysis showed existence of only 3% porosity within the microstructure, indicating a dense coating. Thus, the effect of the porous structure to its mechanical property may be negligible for thermally sprayed Cu coating, which needs further approval. In addition, a good cohesion between copper splats was indicated from the microstructure.

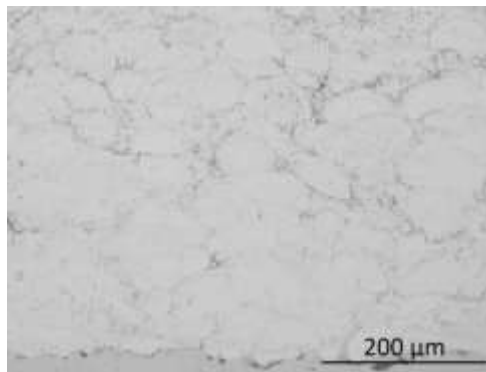


Figure 3 Optical micrograph of copper coating deposited using HVOF technique.

Figure 4(a) shows the SEM image of the Cu-Al Bronze powder (Diamalloy™ 1004) used for thermal spraying. The Diamalloy™ 1004 powder is golden-colored, and fabricated by gas atomization technique in inert gas environment. Table 2 shows the chemical composition of this powder presented by the manufacturer (Oerlikon Metco). Aluminum is considered as major alloying element along with other alloying elements such as iron for this type of bronze alloy.

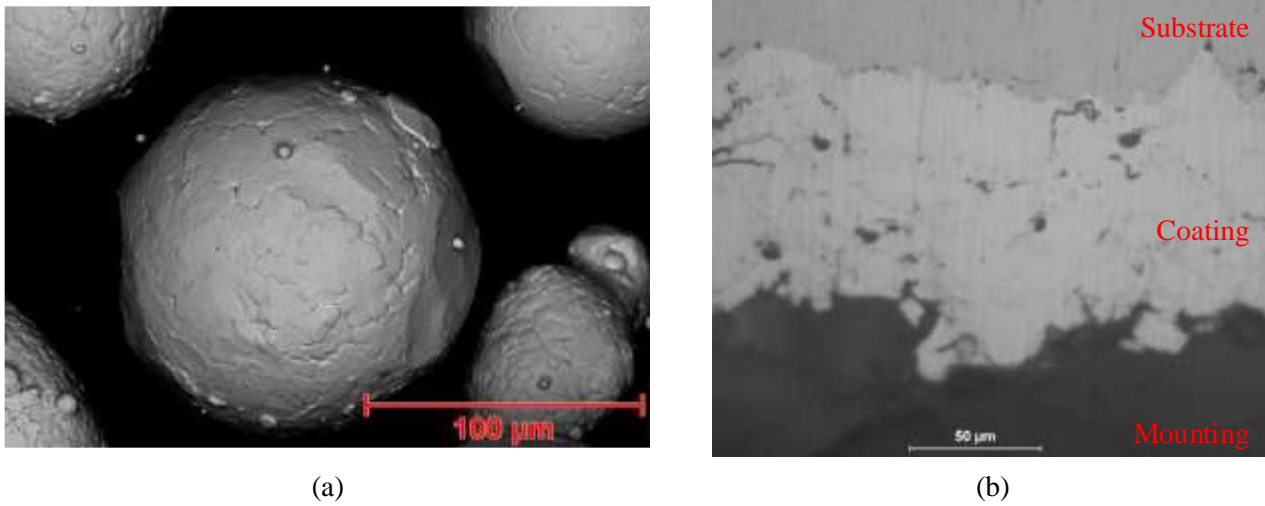


Figure 4 (a) SEM image from Diamalloy™ 1004, and (b) Optical micrograph of HVOF deposited Cu-Al-Bronze coating.

Table 2 Chemical composition of Cu-Al-Bronze powder.

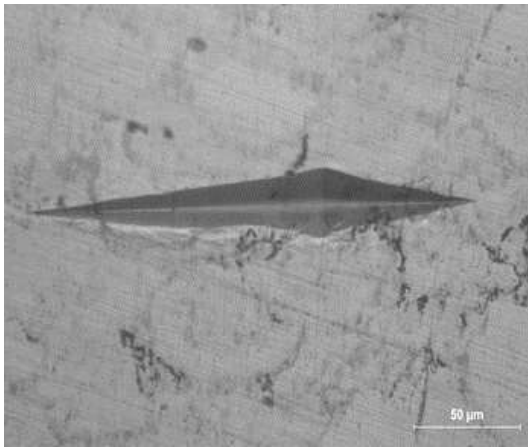
Powder	Cu	Al	Fe	Others (Max)
Diamalloy 1004	Bal	8.5-10.75	0.5-2.0	0.5

Figure 4(b) shows the microstructure of Cu-Al Bronze coating deposited on steel substrate using HVOF technique. The deposited Cu-Al-Bronze coating was dense with no visible delamination which indicated good bonding and adhesion between the coating and the substrate. The thickness of the coating was approximately 90μm. However, as it can be seen in the Figure 4(b), there are several circular and wire shape pores in the coating. According to the data, the porosity level was estimated near $5.5 \pm 1.2\%$ of the cross-section area, which is very small and may also be negligible influence on material mechanical property.

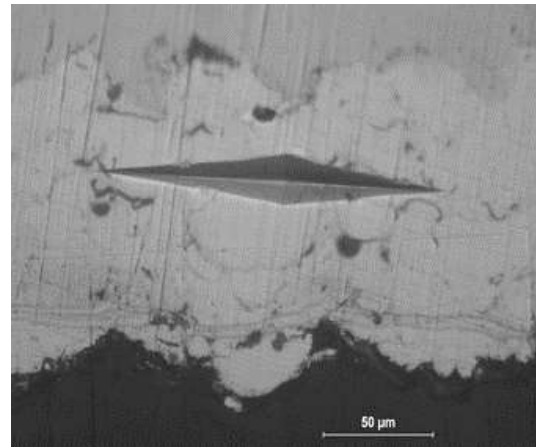
2.3.2 Knoop Micro Indentation Hardness Test

To further investigate the influence of the porosity on mechanical property of the thermally sprayed Cu and Cu-Al Bronze Alloy coatings, the hardness of the two type of coating were tested. The hardness of the two type of coatings were tested using the Knoop Micro indentation test. The Knoop Micro indentation hardness test is a more appropriate test to measure hardness of coating materials. The CLARK CM-800AT machine was specifically used for the testing.

For thermally sprayed Cu coating, hardness tests were performed based on ASTM E2109-01. Figure 5(a) shows the indentation of the Cu coating. The average hardness of the Cu coating is 96.5 HK ($\approx 83\text{Hv}$). For the thermally sprayed Cu-Al Bronze coating, hardness tests were carried out on the coatings cross section based on ASTM E384 -11. Figure 5(b) illustrates the Knoop indentation on Cu-Al Bronze coating. The average hardness of the Cu-Al Bronze coating was estimated near 139.4HK ($\approx 125\text{Hv}$) from 10 hardness measurement which was higher than the Cu coating. Thus, no reduction of mechanical property was identified for the Cu and Cu-Al Bronze coatings.



(a)



(b)

Figure 5 Knoop indentation on HVOF deposited (a) Copper and (b) Cu-Al-Bronze.

2.3.3 Corrosion Resistance Testing Using Electrochemical Approach

After testing the microstructure and hardness of the HVOF deposited coatings of Cu and Cu-Al Bronze, the corrosion resistance of the two different coatings and the bare steel (low carbon steel) were studied and compared. The corrosion performances were tested through accelerated corrosion test using electrochemical method, specifically, the Potentiodynamic Polarization Technique. The accelerated corrosion tests were performed by placing the coated and uncoated steel samples in 3.5% NaCl solutions. A Gamry Reference 600 Potentiostat-Galvanostat-ZRA instrument as shown in Figure 6 had been used to analyze the corrosion performance. Figure 7 shows the corrosion current measured for all the three different materials.



Figure 6 Equipment Set-up for Electrochemical Accelerated Corrosion Test.

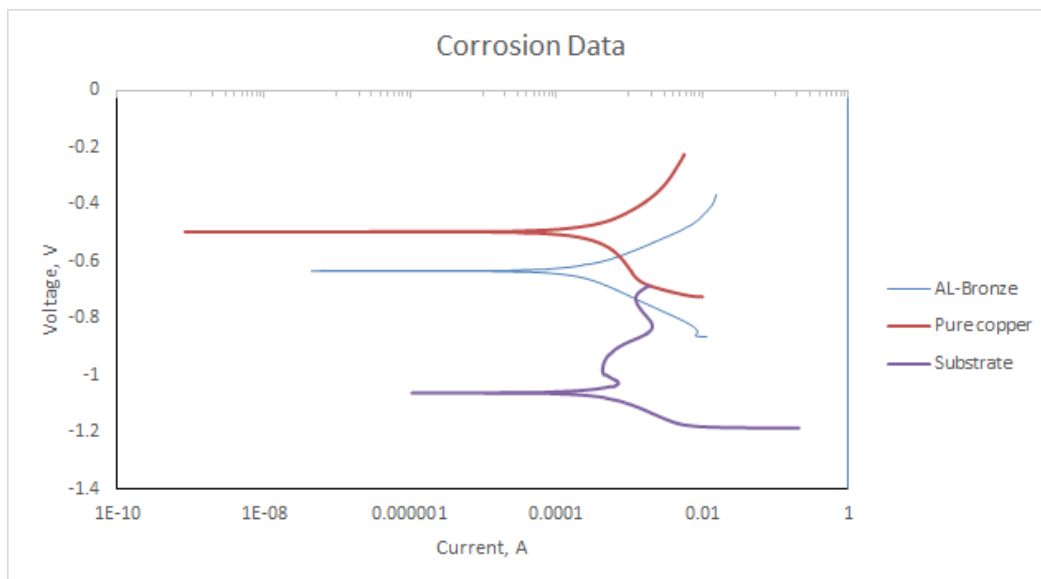


Figure 7 Measured corrosion current for both coated and uncoated samples.

The corresponding electrochemical kinetics parameters such as corrosion potential (E_{corr}), anodic Tafel slopes (β_a) and corrosion current density (I_{corr}) obtained by extrapolation of the Tafel lines are presented in Table 3. The

reduction of corrosion current density of the coatings indicates higher corrosion resistance. For bare steel (low-carbon steel) without coatings, the corrosion current density is $638.3 \mu\text{A}/\text{cm}^2$, and that of the copper coating is $1.956 \mu\text{A}/\text{cm}^2$ and of Cu-Al Bronze is $0.641 \mu\text{A}/\text{cm}^2$, respectively. On the other hand, the increase of corrosion voltage and Tafel slope illustrates an improvement in corrosion resistance. The measured voltage of corrosion and Tafel slope for the uncoated sample are $-1,062 \text{ mV}$ and $4.354 \times 10^{-7} \text{ mV}/\text{dec}$. That for the copper coating are -632.7 mV and $3.74 \times 10^{-3} \text{ mV}/\text{dec}$, while for Cu-Al Bronze they turn out to be -495.1 mV and $5.586 \times 10^{-3} \text{ mV}/\text{dec}$, respectively. According to the corresponding data, corrosion rate of the coatings and the uncoated substrate have also been estimated as shown in Table 3. The uncoated substrate showed a corrosion rate of 18.21 mpy which is typical for low carbon steel, the copper coating showed a corrosion rate of 0.66 mpy, and the corrosion rate for Cu-Al Bronze coating was 0.22 mpy. From Table 3, it can be seen clearly that both Copper and Cu-Al Bronze coatings have a very significant improvement in the corrosion resistance when compared to bare steel without coatings. The Cu-Al Bronze coating not only demonstrated a need for a thinner coating of only $80 \mu\text{m}$ but also showed the best corrosion performance which was three times better than the Cu coating with $800 \mu\text{m}$ which was 10 times thicker than the Cu-Al Bronze coating.

Table 3 Corrosion performance comparison between two different coatings.

Material	Corrosion Potential, E_{corr} (mv)	Corrosion Current Density, i_{corr} ($\mu\text{A}/\text{cm}^2$)	Anodic Tafel Constant, β_a (mV/dec)	Cathodic Tafel Constant, β_c (mV/dec)	Corrosion Rate (mill/year)
Substrate (Bare Low-Carbon Steel)	-1062	638.3	435.4×10^{-9}	104.3×10^{-3}	18.21
Al-Bronze	-495.1	1.956	5.586×10^{-3}	4.923×10^{-3}	0.22
Cu	-632.7	0.641	3.74×10^{-3}	3.39×10^{-3}	0.66

By comparison to the previously reported result for corrosion tests on copper⁴³, it has been drawn that the corrosion resistance of the HVOF deposited copper coating was significantly improved. This achievement in the corrosion behavior of the copper coating can be attributed to the very dense coating with a low level of porosity. According to the data presented for corrosion resistance of Al-Bronze as a coating^{44,45}, it is worth mentioning that, the corrosion resistance of the HVOF deposited Cu-Al Bronze coating has been also marginally improved.

More tests and data analysis were performed on the HVOF deposited Al-Bronze coating samples for a precise measurement and understanding the standard corrosion performance of this material. Table 4 shows the corrected corrosion rate for four HVOF deposited Al-Bronze coated plates with a thickness of $80 \mu\text{m}$. Table 4 shows that the HVOF deposited Al-Bronze coating has an average corrosion rate of 0.3591 mill/year with a variance of 0.0958 mill/year. Compared to a regular uncoated low-carbon steel, which has a corrosion rate of 18.2 mill/year from section 1, a thin layer of thermal sprayed Cu-Al Bronze alloy coating material showed consistent improvement of corrosion resistance.

Table 4 Corrosion performance of Al-Bronze coating.

Sample Number	Anodic Tafel Constant, β_a , (V/decade)	Cathodic Tafel Constant, β_c , (V/decade)	Polarization Resistance ($\text{k}\Omega$)	Corrosion Current (amps)	Corrosion Rate (mill/year)
Sample 1	0.4424	0.1654	3.2	1.636×10^{-5}	0.2953
Sample 2	0.254	0.1499	2.9	1.413×10^{-5}	0.2552
Sample 3	0.5348	0.2047	2.3	2.798×10^{-5}	0.5054
Sample 4	0.5455	0.1806	2.8	2.107×10^{-5}	0.3803

2.4 Summary

In this section, a literature review on thermal spraying coatings were performed by two graduate students, Xiao Liang and S. A. Galedari, to compare the corrosion property of various mettalic thermal spraying coatings such as Al, Zn, and Cu, followed by a systemetic metraisl selection using CES software. Based on these investigation, the graduate students selected copper (Cu) and copper alloys, specifically, Cu and Cu-Al Bronze Alloy, to be used as

thermal spraying materials for corrosion prevention of buried steel pipelines. The material properties of the Cu and Cu-Al Bronze Alloy coatings were tested to approve their effectiveness. They tested the microstructures, hardness, and corrosion resistance of the thermal spraying Cu and Cu-Al Bronze Alloy coatings. The coatings showed to be dense and uniform with porosity less than 5% for both coatings. The hardness tests showed the small porosity of the two coatings did not impact the mechanical property of the coating. The accelerated corrosion tests performed using electrochemical method demonstrated that both Cu and Cu-Al Bronze Alloy coatings improved the corrosion resistance of the steel substrate significantly and a thin layer of HVOF deposited Cu-Al Bronze coating (90 μm) had a better corrosion protection compared to a thicker layer of copper (800 μm).

3 Development of the Self-Sensing Coating System for Corrosion Assessment

To enable the self-sensing capability of the thermally sprayed coatings on steel pipes for corrosion assessment, various sensing techniques were developed and deployed on top of the coating and inside the coatings, including long period fiber grating (LPFG) sensors on the coating surface and fiber Bragg grating (FBG) sensors embedded inside the coating.

3.1 Pipe Surface Environmental Sensing using LPFG based corrosion Sensor

To ensure the effects from the proposed corrosion mitigation system, a corrosion environmental sensing module was also applied using the nano iron/silica particle coated LPFG sensors previously developed by the Co-PI, Dr. Huang's research team⁴⁶. Figure 8(a) shows the shows a typical structure of the LPFG surface corrosion environmental sensor with a particles-filled polymer coating. The black and white dots represent the primary nano iron particles and the nano silica particles, respectively. When placed in a corrosive environment, the embedded iron particles are gradually corroded away, resulting in a change of the sensor's optical properties. The nano silica particles are introduced to improve the transparency of the sensor coating. Together with the polymer, they provide a robust and stable framework of the coating even after all the nano iron particles are corroded completely. Additionally, the polymer coating functions as a buffet/jacket for the LPFG sensor to make it more robust and durable in handling and deployment.

The LPFG based corrosion sensor shown in Figure 8(a) operates by monitoring the corrosion induced optical property change of the coated iron-particle thin film. The effective refractive index of the fiber cladding and the thickness of the coated thin film change when the coated iron particles are corroded. As a result, the resonant wavelength of the LPFG changes correspondingly. Therefore, monitoring of the change in the resonant wavelength of the LPFG sensor provides key information about the mass loss and the material property change of the iron particles over time in a corrosive environment. Figure 8(b) shows the LPFG spectrum changes during its entire fabrication process⁴⁶.

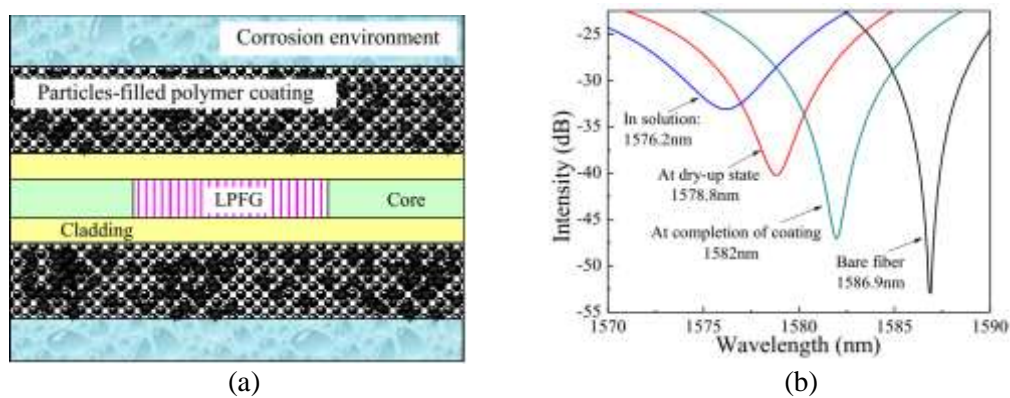


Figure 8 (a) Illustrative structure of an LPFG sensor coated with nano iron particles and (b) LPFG spectrum change during the coating process⁴¹.

3.2 Pipe Corrosion Assessment Using Embedded FBG Sensors inside Coating

3.2.1 Sensor Selection

Fiber Bragg grating (FBG) sensors were selected to be embedded inside the coating due to their unique advantages of non-sensitivity to surrounding chemical environments, compactness, immunity to EMI and moisture, capability of quasi-distributed sensing, and long life cycle, *etc.* Figure 9(a) shows the typical bare FBG sensor (Os1100 from Micro Optics, Inc.), Figure 9(b) shows the reflected light spectrum of a FBG sensor, and Figure 9(c) shows the sensing system setup in Lab for experiments. The NI PXIe-4844 Optical Sensor Interrogator was used in this research for FBG data acquisition. Before embedding the fiber optic sensors inside the coating through the thermal spraying coating process, sensor calibration tests were performed before embedment including strain and temperature calibrations.

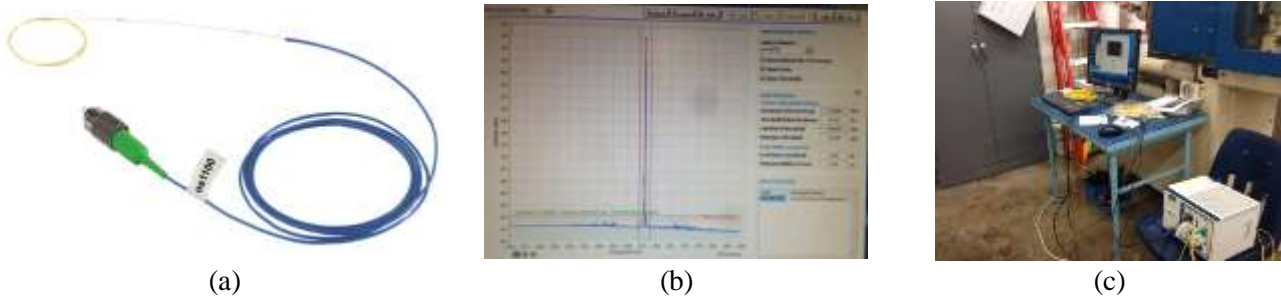


Figure 9 (a) Typical FBG (Os1100), (b) reflected spectrum, and (c) sensing system setup in Lab.

3.2.2 Sensor Calibration

The FBG sensors (both strain and temperature sensors) used in this project were purchased from Micro Optics, Inc. Sensor calibrations for strain (Os1100) and temperature (Os4200) have been performed in Lab. Figure 10 and Figure 11 show the strain and temperature calibration of the fiber optic sensor, respectively. As shown in Figure 10 for s repeated strain sensing of two times, the FBG strain sensor has a strain sensitivity of $1.07\text{pm}/\mu\epsilon$. Figure 11 shows that the temperature sensitivity is around $9.5\text{pm}/^\circ\text{C}$ in room temperature. Due to the large temperature sensitivity, a temperature sensor is needed on the side of the strain sensor to compensate the temperature effects.

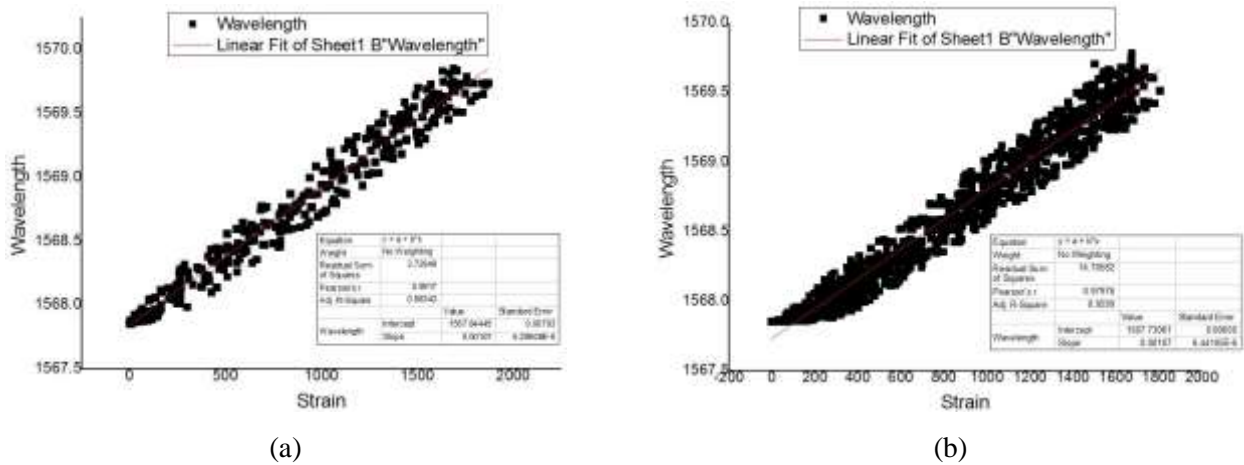


Figure 10 Results from strain calibration test (a) test #1 and (b) test #2.

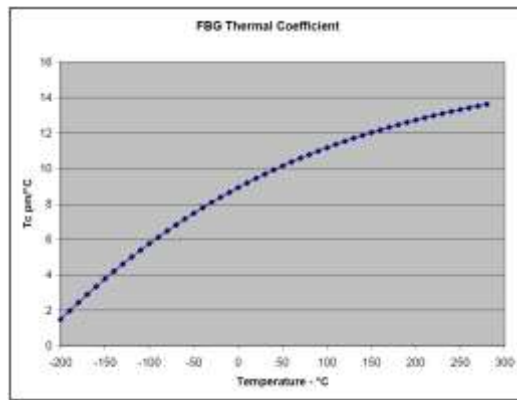


Figure 11 Results collected from temperature calibration test (Courtesy of Micro Optics, Inc.).

3.2.3 Sensor Embedment

Taking into consideration that the HVOF process which induces high pressurized air could result in damaging the sensors during spraying, an effective protection must be provided for sensors during spraying process. Several protection techniques have been proposed in this project: 1) strain sensors were protected using steel (OS 3100) and attached to the test sample using glues as shown in Figure 12(a) for the sample and Figure 12(b) shows the deposition set-up; 2) permanent protection by protecting strain sensor through steel tubes inside a shallow groove in addition to adhesives for embedment (shown in Figure 13). For the second plan, three different types of high-temperature adhesives have been investigated, including i) epoxy-based (Minco #15 Epoxy, two samples), ii) metallic-nickel-based (Durabond 952 from Cotronics Corp., one sample), and iii) metallic-stainless steel-based (Durabond 954 from Cotronics Corp., one sample) adhesives as shown in Figure 14(a) ~ Figure 14 (c), respectively.

HVOF spraying results showed that first plan ended up with a broken strain sensor. Noticeable fiber breakage was notified at the strain sensor as cycled out in Figure 15. The sensor reading indicated that the sensor was no longer working after 3 rounds of spraying (Figure 16).

For the second plan, it is worth mentioning that surface of all the tests samples were sandblasted before spraying to increase coating adhesion to the substrate as shown in Figure 17(a~c), respectively. As shown in Figure 17 (b), after sand-blast, the protection ii) nickel-based adhesive failed right after sandblasting process. Thus, the sample with nickel based metallic adhesive was eliminated for further spraying coating. The rest three test samples (two samples with epoxy and one sample with stainless-steel-based adhesive) were put ahead for spraying coating as shown in Figure 18(a). Figure 18(b) shows the samples after coating for the reason of comparison.

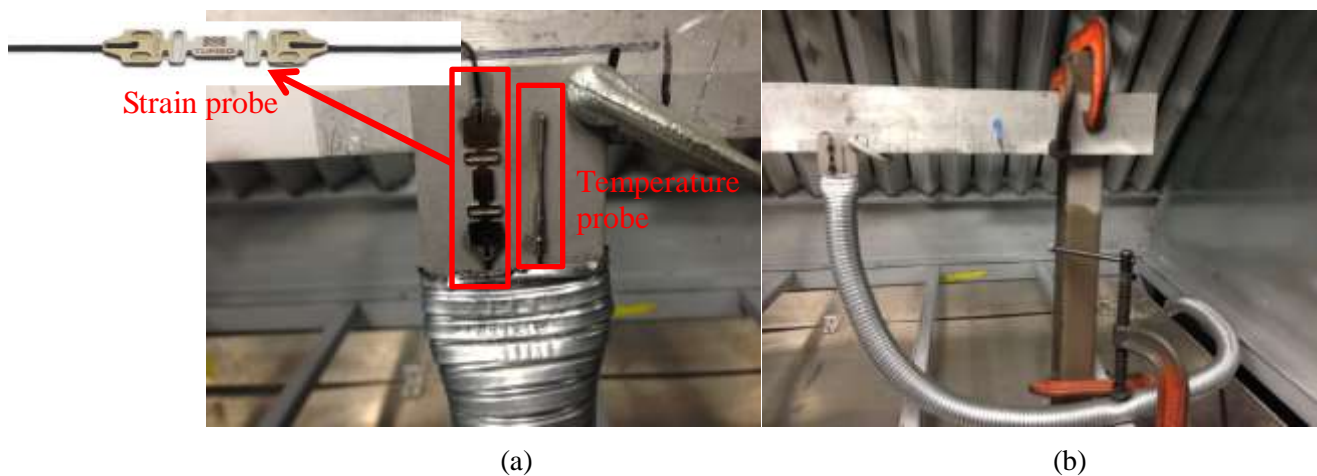


Figure 12 Sensor set-up for HVOF coating deposition (a) sensors position on the substrate and (b) deposition coupon set-up.

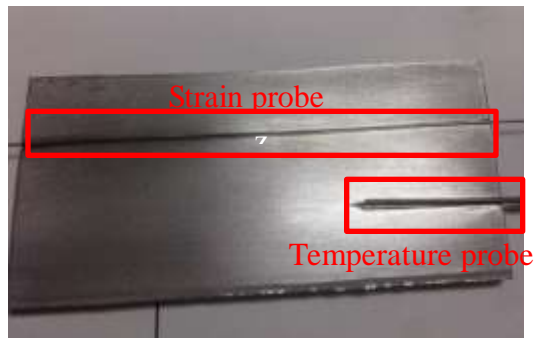


Figure 13 Temporary protection for sensors as second technique used in this project.

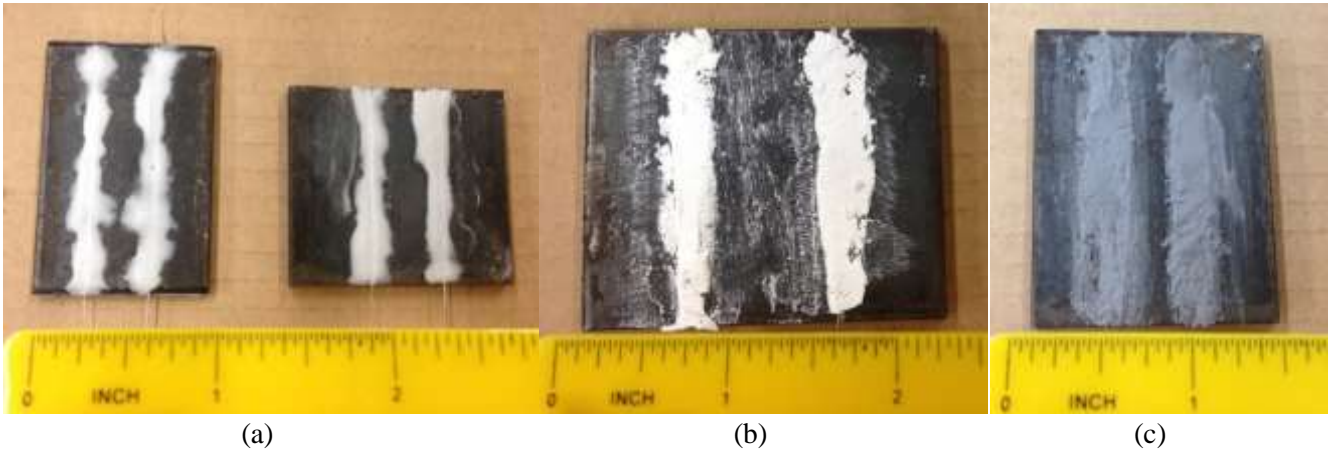


Figure 14 Coated samples using (a) high temperature epoxy (Minco Epoxy), (b) nickel-based metallic adhesive (Durabond 952), and (c) stainless-steel-based metallic adhesive (Durabond 954).

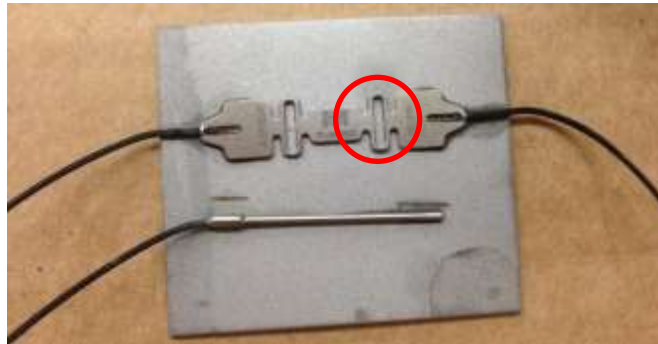


Figure 15 Strain sensor after spray process in plan 1).

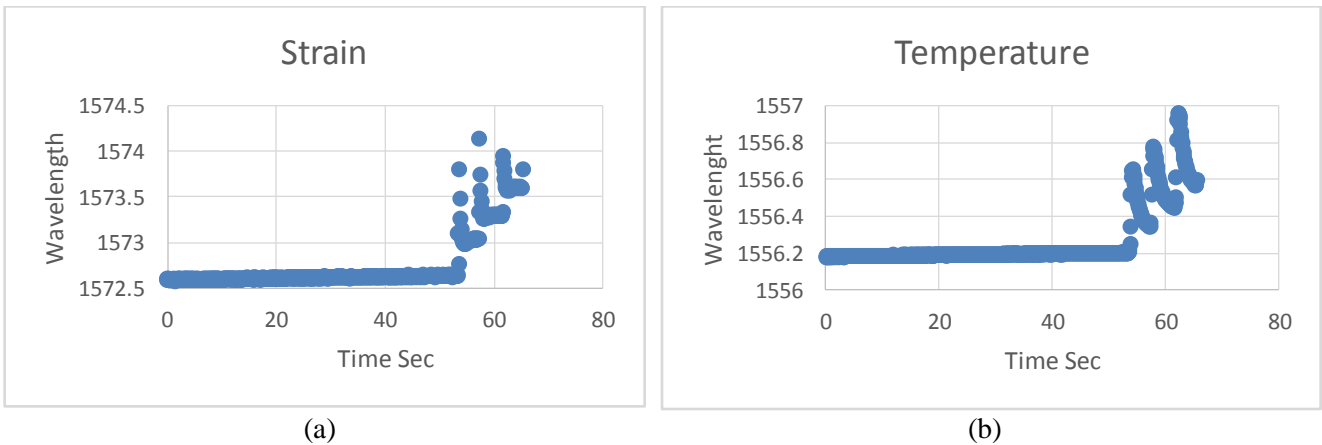


Figure 16 Collected wavelengths during the second run of spraying (a) strain and (b) temperature.

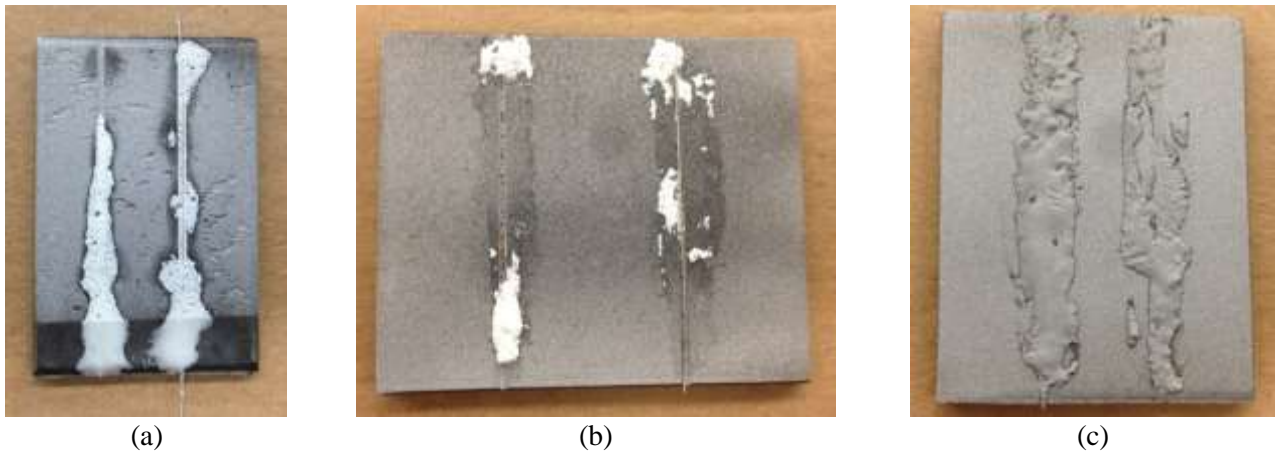


Figure 17 Coated samples after sand blasting process (a) high temperature Minco Epoxy, (b) nickel-based adhesive (Durabond 952), and (c) stainless-steel-based adhesive (Durabond 954).

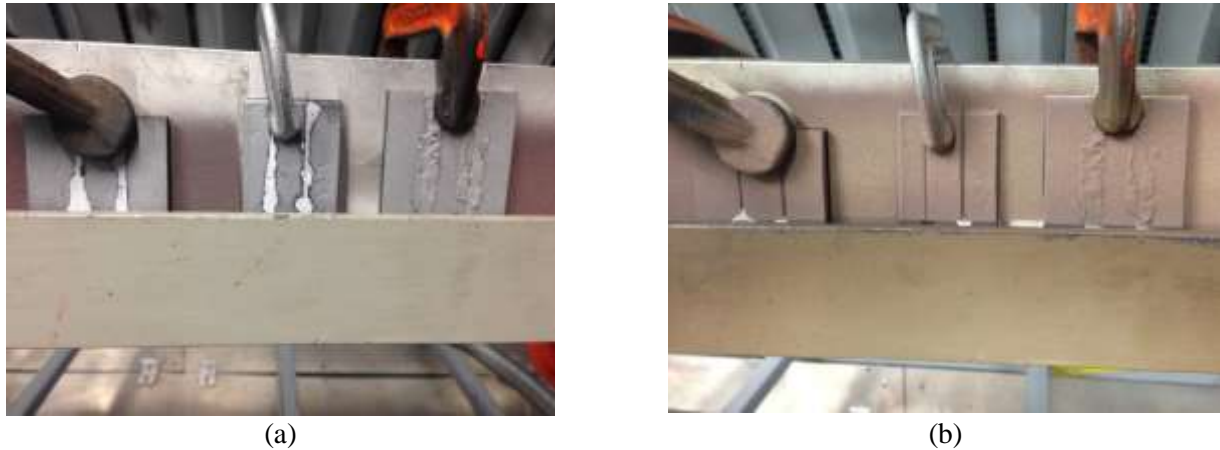


Figure 18 (a) Spraying samples for various adhesive before coating and (b) after spraying deposition.

Figure 19(a) and (b) show a more detail view at higher magnification of three samples after HVOF spraying process. The stainless-steel-based metallic adhesive successfully survived the thermal spray coating process as shown in Figure 19(b). The copper coating was successfully deposited on top of the adhesive and sensor at the thickness of 0.55 mm. Microstructure of the deposited coating and its thickness is shown in Figure 19(c). The optimization of the stainless-steel-based metallic adhesive embedded coating will be performed to make a smoother surface of the adhesive and test its sensing behavior after coating deposition.

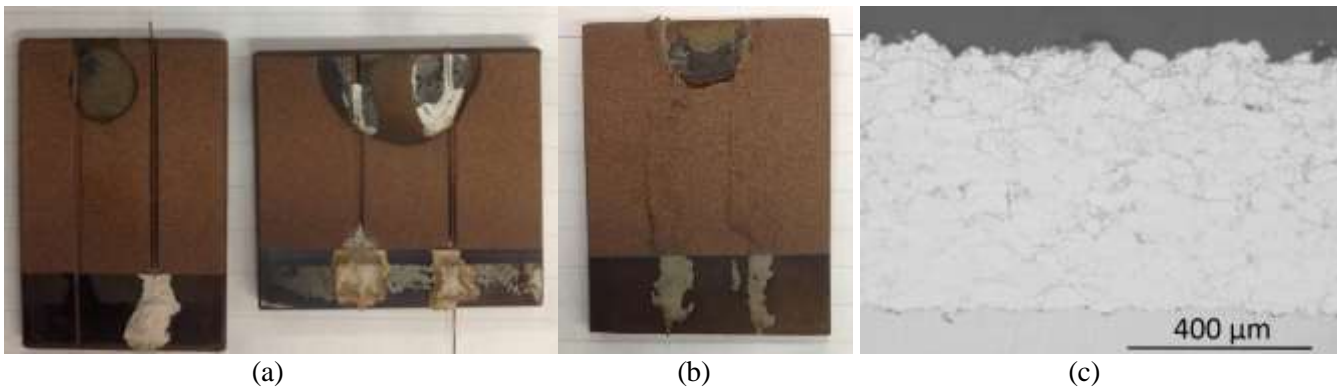


Figure 19 Sample condition after coating deposition (a) with high-temperature epoxy, (b) with stainless-steel-based metallic adhesives, and (c) cross-section of thermally deposited copper coating

3.3 Summary

In this section, the thermally sprayed coatings were enabled for self-sensing both for corrosion environments and its own corrosion performance by the two graduate students, Xiao Liang and S. A. Galedari, and one postdoc, Dr. M. SalimiJazi. A nano iron particle dispersed polymer coated LPFG sensor was developed to detect the corrosion environments of the steel pipe on its surface. More importantly, a FBG based sensing system was

embedded inside the thermal spraying coating for corrosion assessment. Studies showed bare FBG sensors packaged with steel tubes and attached using stainless-steel-based metallic adhesives, can survive the harsh environments during the thermal spraying coating process, resulting in an effective embedment technique for the proposed self-sensing coating.

4 Corrosion Experiments and Results on Steel Bars

To approve the effectiveness of the developed LPFG sensors for corrosion environmental monitoring of steel pipes, in this section, accelerated corrosion tests were performed on steel bars using both the developed sensors and the traditional electrochemical method.

4.1 Sample Preparation

Steel bar was selected as the investigating subject in this study to investigate the LPFG based surface corrosion environmental sensor. Figure 20 shows the preparation of the test steel bars^{46, 47}. With 0.383% carbon contained in the steel bar, the test specimen was categorized as mild carbon steel. To get a uniform corrosion in the middle of the bar, epoxy was applied to both ends of the steel rebar by placing the epoxy into a small section of PVC tubes. Channels on the surface of the steel bars were prepared for the installation purpose of the coated LPFG corrosion sensors and the associated environmental referencing LPFG sensors. At one end of the steel bar, electrical wires were installed to monitor the corrosion rate through traditional electro-chemical methods, in which a potentiodynamic test was implemented for the test steel bar for a corrosion rate estimation.



Figure 20 Prepared steel rebar samples for corrosion testing.

4.2 Experiment Setup

The three steel bars were placed inside a 3.5 wt.% NaCl solution. Two measurement methods were applied to monitor the corrosion of the steel bar samples including the optical and electrochemical measurements as shown in Figure 21(a, b). Three nano iron/silica particle coated LPFG sensors and one reference sensor were attached on the surface of the steel bar to monitor the corrosion together with the electrochemical methods.

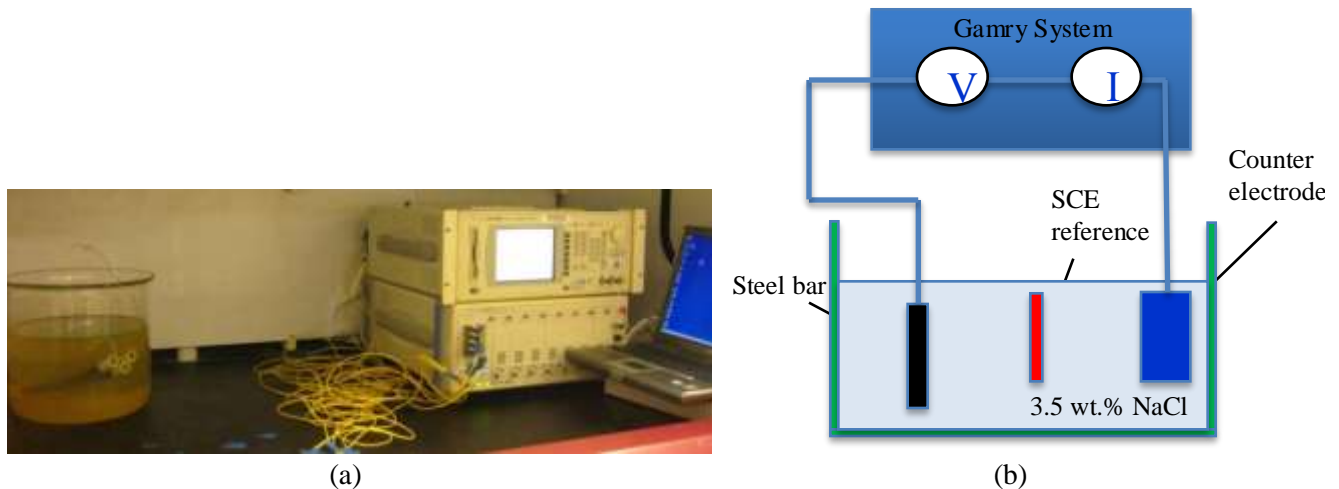


Figure 21 Experimental setups for corrosion monitoring of three steel bars (a) for optical and (b) for electrochemical measurements.

4.3 Data Analysis

The tests were performed for 20 days (480 hours). Figure 22(a) illustrated the spectrum changes of the sensor. Figure 22(b ~ d) show the center wavelength changes of the reference sensor, the corrosion environmental sensor after reference correction, and the light intensity changes of the corrosion environmental sensor. As the immersion time increased, both the resonant wavelength and the peak intensity of the coated LPFG#1 sensor first increased rapidly and then approached an asymptotical value. Specifically, the resonant wavelength dramatically changed from 1573.3 nm to approximately 1580.2 nm during the first two weeks of laboratory corrosion tests, whereas most of the change in peak intensity from -40.5 dB to -20 dB occurred within the first three days of corrosion tests. Similar responses were observed for the other two samples as indicated in Figure 23(a, b).

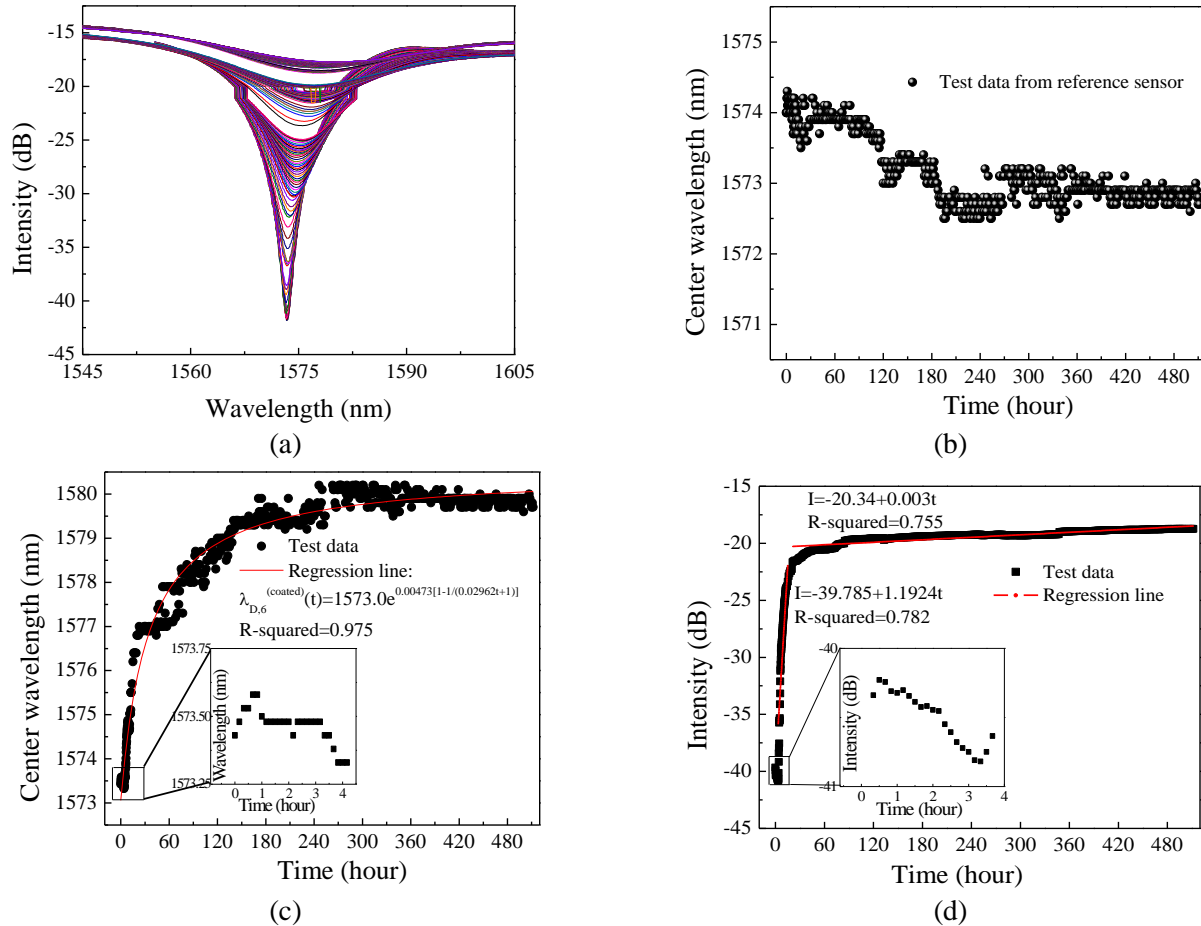


Figure 22 Spectrum changes of the surface corrosion environmental sensor in 3.5% salt solution for (a) one month, (b) center wavelength changes of reference sensor, (c) compensated center wavelength changes, and (d) light intensity changes of the surface corrosion environmental LPFG sensor #1.

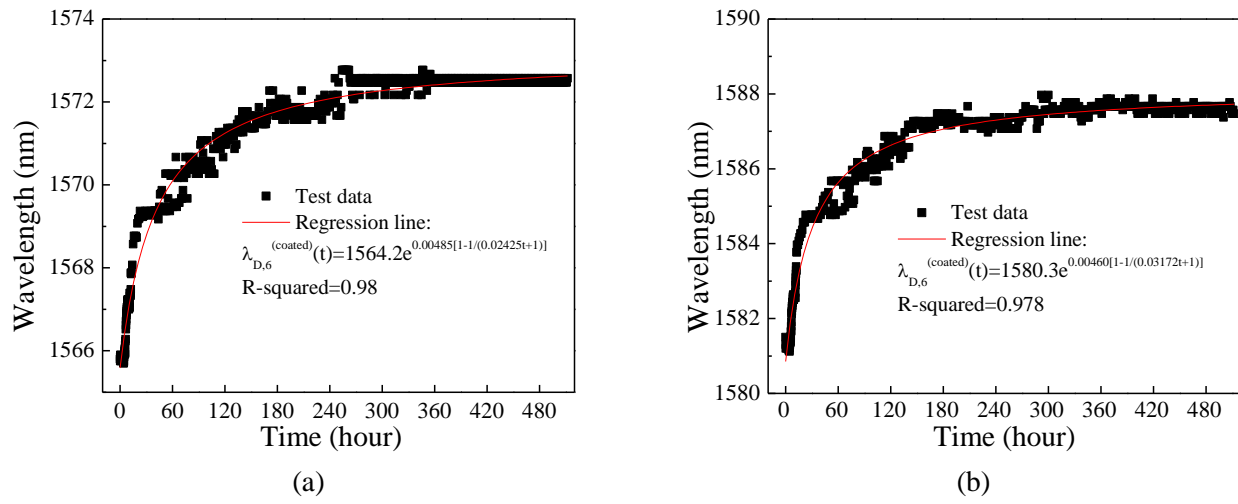


Figure 23 Compensated center wavelength changes of (a) LPFG #2 and (b) #3.

At the beginning of corrosion test when $t = 0$, the difference in resonant wavelength and the coating thickness were equal to 6.9 nm and 3.5 μm according to previous study, respectively. Therefore, for sensors with the same design as the calibration LPFG sensors previously, the sensors' wavelength changes towards the coating thickness changes can be represented as:

$$\frac{\lambda_{D,6}^{(reference)}(t) - \lambda_{D,6}^{(coated)}(t)}{6.9} = \frac{d_{coating}(t)}{3.5} \quad (6)$$

in which $\lambda_{D,6}^{(reference)}(t)$ and $\lambda_{D,6}^{(coated)}(t)$ represent the resonant wavelengths of the reference and coated LPFG sensors, respectively; t denotes the immersion time of sensors in 3.5wt.% NaCl solution; and $d_{coating}(t)$ is the coating thickness at any time t .

The corrosion rate of the steel bar was also measured using electrochemical method. Figure 24 shows the measured results for the three steel bars. The predicted corrosion rates using Equation (5) by three LPFG sensors and the measured corrosion rates by potentiodynamic tests, were compared in Table 5 together with their differences. The developed surface sensor measured the corrosion rate to be 0.0373mm/year and that from the electrochemical method were 0.0345mm/year. Table 5 also listed the average and the coefficient of variation (C.O.V.). The corrosion rates obtained from the potentiodynamic tests were for the mass loss of three steel samples. The corrosion rates obtained from the three LPFG sensors were for the mass loss of nano iron particles on the sensors after 130.5 hours of immersion time. It can be observed from Table 5 that the maximum difference between the LPFG prediction and its corresponding potentiodynamic measurement was 0.0087 mm/year, corresponding to a relative error of $0.0087/0.0295=29\%$. The average difference was 0.0028 mm/year, corresponding to a relative error of $0.0028/0.0345=8\%$. This comparison validated the accuracy of the proposed sensing technique for steel corrosion monitoring. In addition, the C.O.V. values of the three predicted and their corresponding measured corrosion rates were 0.049 and 0.115, respectively. These results indicated that the proposed sensing technology was more repeatable and reliable than the potentiodynamic tests in terms of the evaluation of corrosion rate.

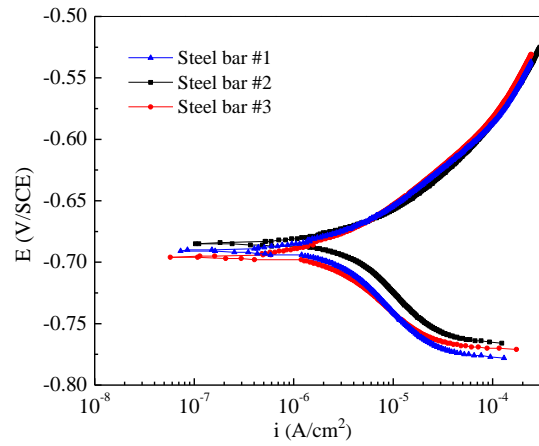


Figure 24 Monitored potentiodynamic polarization curves for the three test samples.

Table 5 Mass loss comparison from LPFG sensors and potentiodynamic tests.

Test sample (LPFG/steel bar)	$\frac{dd_{coating}(t)}{dt}$ (mm/year)	LPFG sensors (mm/year)	Potentiodynamic tests (mm/year)	Difference (mm/year)
#1	$\frac{0.9011}{(0.02962t+1)^2} e^{0.00473 \times (1 - \frac{1}{0.02962t+1})}$	0.0348	0.0348	0
#2	$\frac{0.7421}{(0.02425t+1)^2} e^{0.00485 \times (1 - \frac{1}{0.02425t+1})}$	0.0390	0.0392	-0.0002
#3	$\frac{0.9682}{(0.03172t+1)^2} e^{0.00460 \times (1 - \frac{1}{0.03172t+1})}$	0.0382	0.0295	+0.0087
Average	N/A	0.0373	0.0345	+0.0028
C.O.V.	N/A	0.049	0.115	+1.464

4.4 Summary

In this section, the effectiveness of the LPFG surface corrosion environmental sensors were tested by the graduate student, Xiao Liang, and his advisor, Dr. Ying Huang, using accelerated corrosion tests on steel bars. Three steel bars attached with the developed LPFG surface sensors were tested. The developed surface sensor measured the corrosion rate to be 0.0373mm/year and that from the electrochemical method were 0.0345mm/year. The C.O.V. values measured from the developed surface sensor and the electrochemical method were 0.049 and 0.115, respectively. It validated the accuracy of the developed sensing technique for steel corrosion monitoring, indicating that the developed surface sensor was more repeatable and reliable than the potentiodynamic tests in terms of the evaluation of corrosion rate.

5 Corrosion Experiments and Results on Steel Plates

As stated in Section 3.2.3, challenges of FBG sensor embedment were resolved by applying stainless-steel-based metallic adhesive (Durabond 954) in combination of steel tube and it was approved that the adhesive can survive the coating process. In this section, accelerated corrosion tests were performed on the embedded FBG sensing system for corrosion assessment to approve its effectiveness.

5.1 Sample Preparation

5.1.1 Pre-spray Preparation Process

In this corrosion assessment experiment, a total of ten steel plate samples were prepared using Cu-Al Bronze coating for further investigation of corrosion characteristics, including four samples with embedded sensors and thermal sprayed coating (Sample 1~4), two samples without thermal coating but with embedded sensors (Sample 5~6), two reference samples with thermal sprayed coating but without embedded sensors (Sample 7~8), and two samples without any thermal sprayed coating (Sample 9~10).

Figure 25 shows the samples with embedded sensors ready for HVOF process. The dimensions were 8 (length) \times 4 (width) \times 0.25 (thickness) inches. A small groove has been made in each sample to embed fiber optic sensors inside the samples. The sensors were enclosed in hypodermic tubes for protection and embedded using stainless-steel-based metallic adhesive (Durabond 954).



Figure 25 Steel substrate prepared in this quarter with embedded sensors before spraying process.

Figure 26 (a ~ c) show the accurate location of embedded sensors in all four coated samples. To ensure a successful protection of the fiber optic strain sensors during the HVOF process, hypodermic tubes at two different sizes were used here. A smaller-diameter hypodermic tube was used to protect the sensing unit with 0.006 in. of inner diameter and 0.010 in. of outer diameter. A slightly larger diameter hypodermic tube was used to protect the communication optical fibers from the high speed velocity of HVOF thermal spraying process with an inner diameter of 0.028 in. and an outer diameter of 0.0425 in. For fiber optic temperature sensor, since a relative thicker steel tube was applied by manufacturers for sensor protection, no future protection was taken. As shown in Figure 26, therefore, in samples #1 to #3, each sample had one embedded fiber optic strain sensor (OS1100 single FBG sensor). In sample #4, one fiber optic strain sensor (OS1100 single FBG sensor) and one fiber optic temperature sensor (OS4210 FBG temperature sensor) were placed for temperature monitoring during thermal spraying process which will also be used as reference for corrosion monitoring in future corrosion testing. Figure 27(a) shows all the prepared samples and Figure 27(b) shows the samples after sand blasting process. As it can be seen from Figure 27(b), only the top half of the samples where the sensors located will be coated by Cu-Al Bronze alloy.

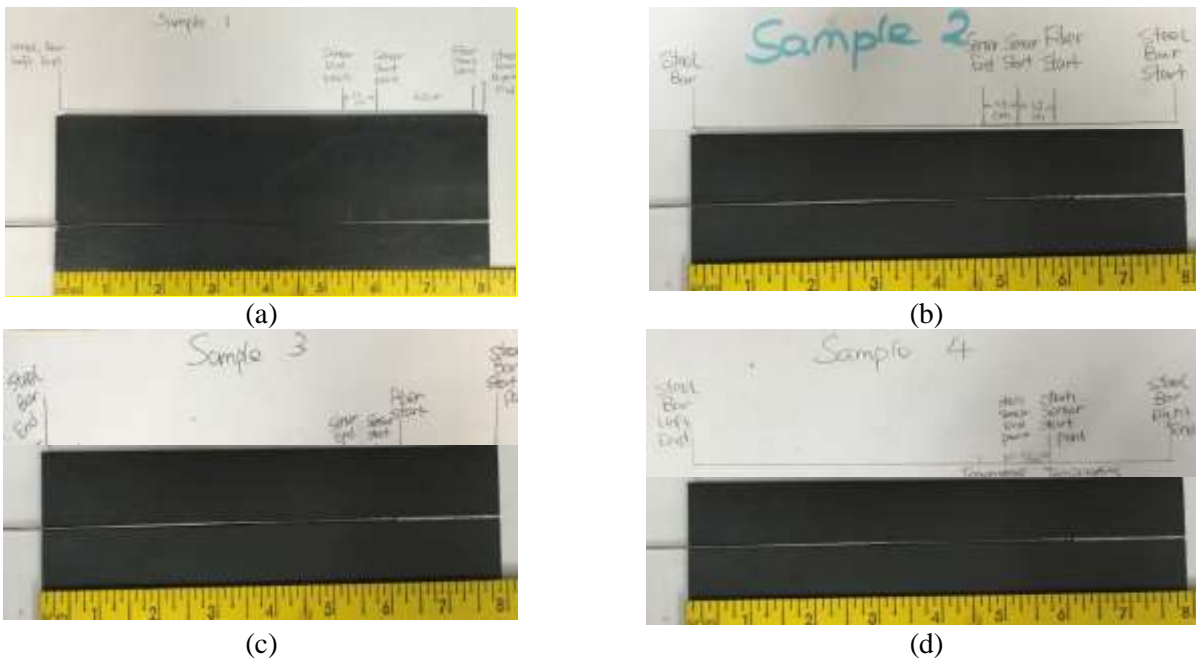


Figure 26 (a-d) Sample preparation with sensor location for Sample #1- 4.



(a)



(b)

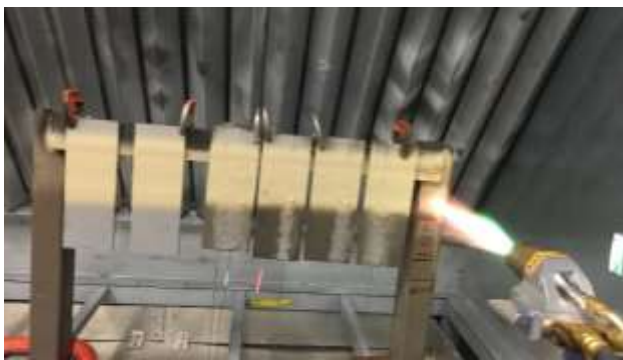
Figure 27 (a) Prepared samples after sensor embodiments, and (b) after sand blasting.

5.1.2 Thermal Spraying Coating for Samples

The prepared samples were then thermal sprayed by Cu-Al Bronze alloy as shown in Figure 28(a ~ b) for the sample setup and thermal spraying process using automatic robotic spraying arms. A total of six traverses were made for the thermal spraying coating and Figure 28 (b) shows the samples after successful thermal spraying. The responses of the sensors on Sample #2 ~ #4 were fully recorded during the thermal spraying process. Figure 29(a ~ c) show the fiber optic strain sensors' responses and Figure 29(d) shows the fiber optic temperature sensor's response. All the sensors successfully survived the thermal spraying coating process and monitored the coating process. The six traverses were clearly demonstrated in all the sensor readings. With the temperature increases during the spraying process, all the sensors performed similarly with respect to temperature changes.

Table 6 compared the sensors' change after the spraying process. From Section 3.2.2, it was known from the sensor's calibration that the strain sensor has a strain sensitivity of $1.07 \text{ pm}/\mu\epsilon$ and the temperature sensor has a sensitivity of $9.5 \text{ pm}/^\circ\text{C}$. Therefore, an analysis of the center wavelength changes of the sensors had been performed.

Table 7 listed each sensor's responses right after coating and after cooling. An average center wavelength change of 1.425 nm was observed during the coating process for the fiber optic strain sensors and a center wavelength change of 0.663 nm was observed for the temperature fiber optic sensor. It is indicated that an average of thermal strain of $1,329 \mu\epsilon$ and a temperature increase of $70 \text{ }^\circ\text{C}$ was introduced by the elevated temperature during the coating process. After cooling down, the environmental temperature drops $6.3 \text{ }^\circ\text{C}$ before the coating and the coating had a thermal residual strain of an average of $192 \mu\epsilon$ in compression with the entire processes considered.



(a)



(b)

Figure 28 (a) Thermal spraying process and (b) Samples after successful thermal spraying.

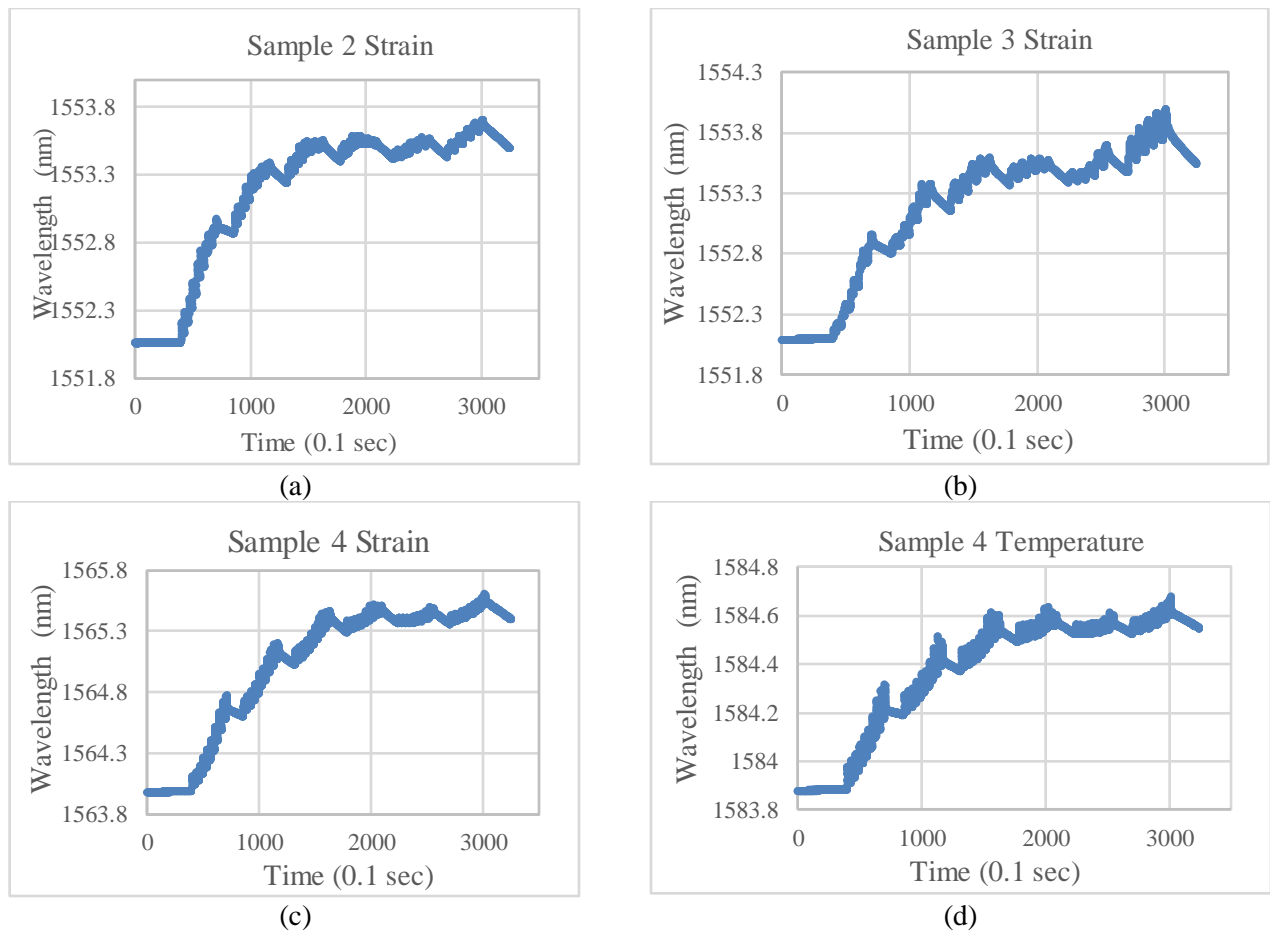


Figure 29 Sensor recording during the thermal spraying process for (a) Sample #2, (b) Sample #3 (c) Sample #4 strain sensor and (d) Sample #4 for temperature sensor.

Table 6 Sensor responses towards the HVOF thermal spraying coating process

Sample No.	FBG Sensor Type	Center Wavelength before Coating (nm)	Center Wavelength right after Coating (nm)	Center Wavelength after coating Cooling (nm)
#2	OS1100 strain sensor	1552.064	1553.496	1551.812
#3	OS1100 strain sensor	1552.109	1553.544	1551.665
#4	OS1100 strain sensor	1564.002	1565.402	1563.874
#4	OS4210 Temperature sensor	1583.887	1584.55	1583.827

Table 7 Sensor response calculations.

Sample No.	Wavelength Change right after Coating (nm)	Strain/Temperature Change ($\mu\epsilon$; $^{\circ}\text{C}$)	Wavelength Change after Coating Cooling (nm)	Strain or Temperature Change ($\mu\epsilon$; $^{\circ}\text{C}$)	Residual Strain Change after Temperature Compensation
#2 strain	1.432	1,338 $\mu\epsilon$	-0.252	-235.5 $\mu\epsilon$	-179.4 $\mu\epsilon$
#3 strain	1.435	1,341 $\mu\epsilon$	-0.444	-415.0 $\mu\epsilon$	-331.0 $\mu\epsilon$
#4 strain	1.4	1,308 $\mu\epsilon$	-0.128	-119.6 $\mu\epsilon$	-66.5 $\mu\epsilon$
#4 temperature	0.663	69.8 $^{\circ}\text{C}$	-0.06	- 6.3 $^{\circ}\text{C}$	0 $^{\circ}\text{C}$

5.2 Electrochemical Accelerated Corrosion Test and Results

In addition to the embedded sensors, electrochemical method was also used to assess the corrosion rate of the coated samples. The Gamry Reference 600 Potentiostat-Galvanostat-ZRA instrument, which is the same instrument as used in Section 03 (shown in Figure 21), had been used to analyze the coated samples. To have the sample coated surface submerged in 3.5% NaCl solution, PVC pipes were glued using Loctite epoxy on the coated surface

for hosting the testing solution. The diameter of PVC pipe was approximately 40.5 mm as shown in Figure 30(a) for uncoated sample with embedded sensors and Figure 30(b) for coated sample with embedded sensors. A 24-hour curing time in room temperature was used to let the adhesive reaching its maximum strength.

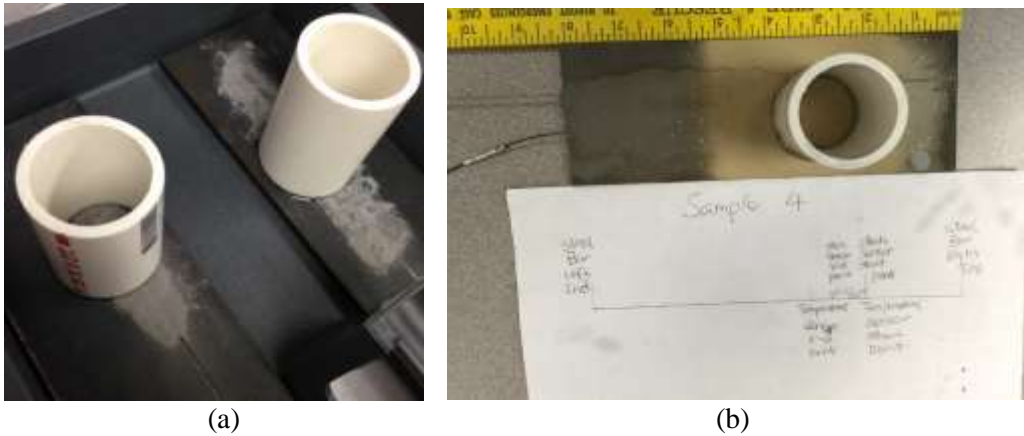


Figure 30 (a) A PVC glued uncoated and (b) coated samples with embedded sensor ready for corrosion tests.

After preparation of the test set-up, 3.5wt.% NaCl solution was poured in the PVC pipes for electrochemical accelerated corrosion tests in an enclosed space. Proper connections must be provided as shown Figure 31.

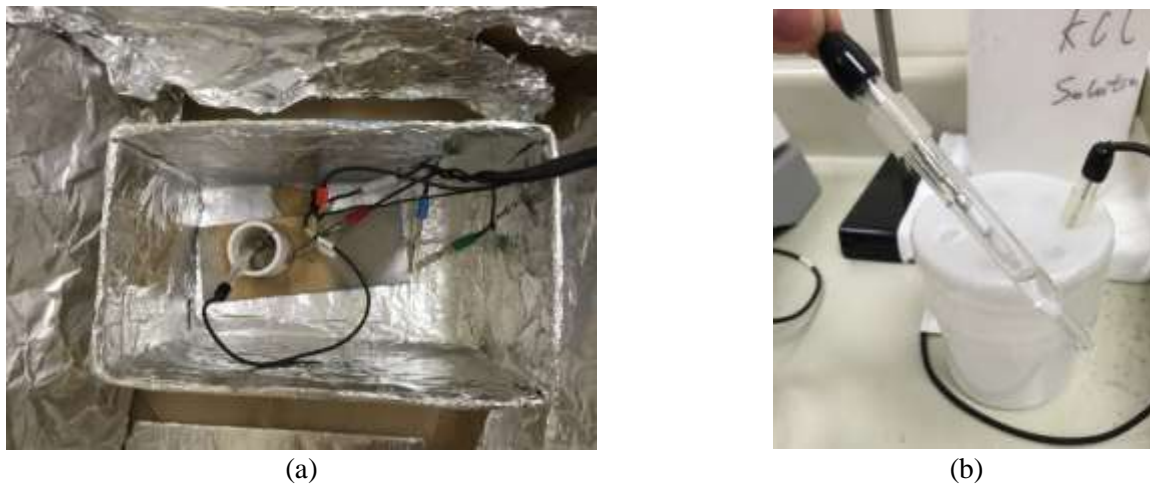
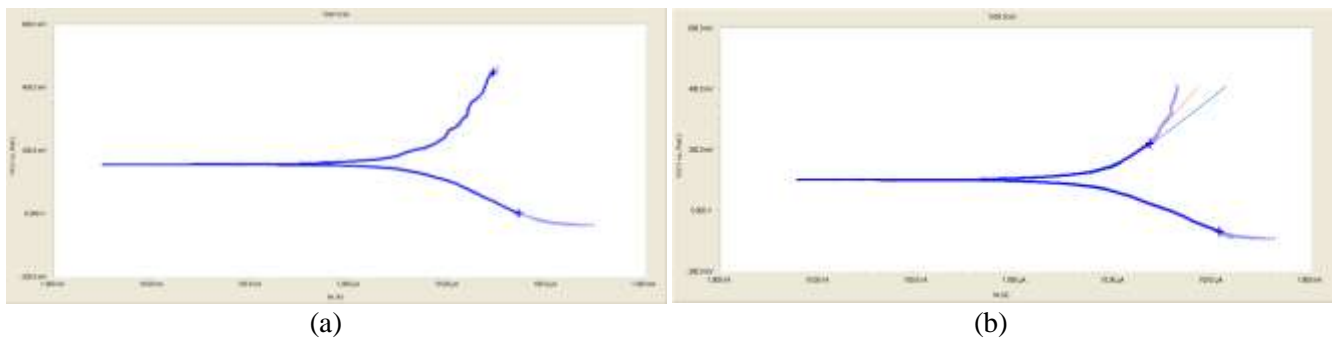


Figure 31 (a) Electrochemical accelerated corrosion test setup and (b) Electrodes used in tests.

After proper connection between leads and samples, the polarization resistance test was performed on all the four coated samples with embedded sensors. The area, density, and equivalent weight of samples were measured and input into the software for testing. All the test procedures were strictly following the standard of ASTM G59 manual. With the polarization resistance, the Tafel tests were performed for each sample. Figure 32(a~d) show the voltage (in Y axis) versus log-scale current (in X axis) for the four samples with embedded sensing system, respectively.



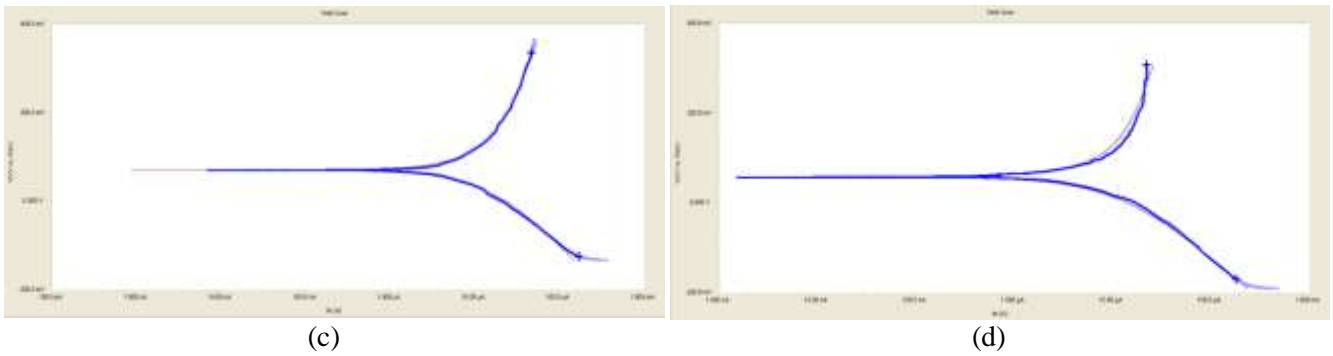


Figure 32 Voltage vs current changes from Tafel tests for (a) Sample #1, (b) Sample #2, (c) Sample #3, and (d) Sample #4.

The β_a and β_c in Equation (3) had been calculated for each sample (generally the β_a varies from 0.06 to 0.12 V/decade, and the β_c varies from 0.06 to infinity). The corrosion rate of each of sample was calculated according to Equation (4) as shown in Table 8. Since Sample #3 had a pre-testing corrosion due to unintended explosion to moisture, its corrosion rate is relatively larger than the rest three samples, which will not be included in the analysis. The three thermal sprayed hard coating samples have an average corrosion rate of 8.85×10^{-2} mill/year with standard derivation of 2.84×10^{-2} mill/year. Compared to the uncoated steel, which has an average corrosion rate of 1 mill/year from the testing of the two uncoated samples in this study, a thin layer of thermal sprayed hard coating with $50\mu\text{m}$ significantly improved the corrosion resistance of the steel substracts by more than 10 times.

Table 8 Test results from electrochemical chemical methods.

Sample Number	Anodic Tafel constant β_a , V/decade	Cathodic Tafel Constant β_c , V/decade	Corrosion Rate mill/year
Sample 1	0.4424	0.1654	8.550×10^{-2}
Sample 2	0.254	0.1499	6.709×10^{-2}
Sample 3	0.5348	0.2047	10.508×10^{-2}
Sample 4	0.5455	0.1806	9.636×10^{-2}

5.3 Accelerated Corrosion Test for Steel Plates Using Embedded Sensing Systems

After the accelerated corrosion tests using electrochemical methods, another series of corrosion tests were performed on the four samples with embedded in-line FBG sensors by emerging them in PVC tubes filled with 3.5% NaCl solution for 21 days. The wavelength changes of four samples had been recorded continuously for entire test time with a sampling frequency of 10Hz. Figure 33(a~d) show the photos had been taken of each sample every day for seven days for visual inspection. Comparison of the visible changes in the samples as seen in Figure 33 helps to better understand the corrosion propagations. For Sample #2 and Sample #4, the corrosion area is exactly above the embedded sensors. The corrosion area of Sample #1 is close to the embedded sensor but not exactly right above it. Since Sample #3 had been corroded before corrosion test, the corrosion area is larger than other samples. The corrosion area was increased rapidly, and it was shadowed which represents the magnitude of corrosion level is serious.

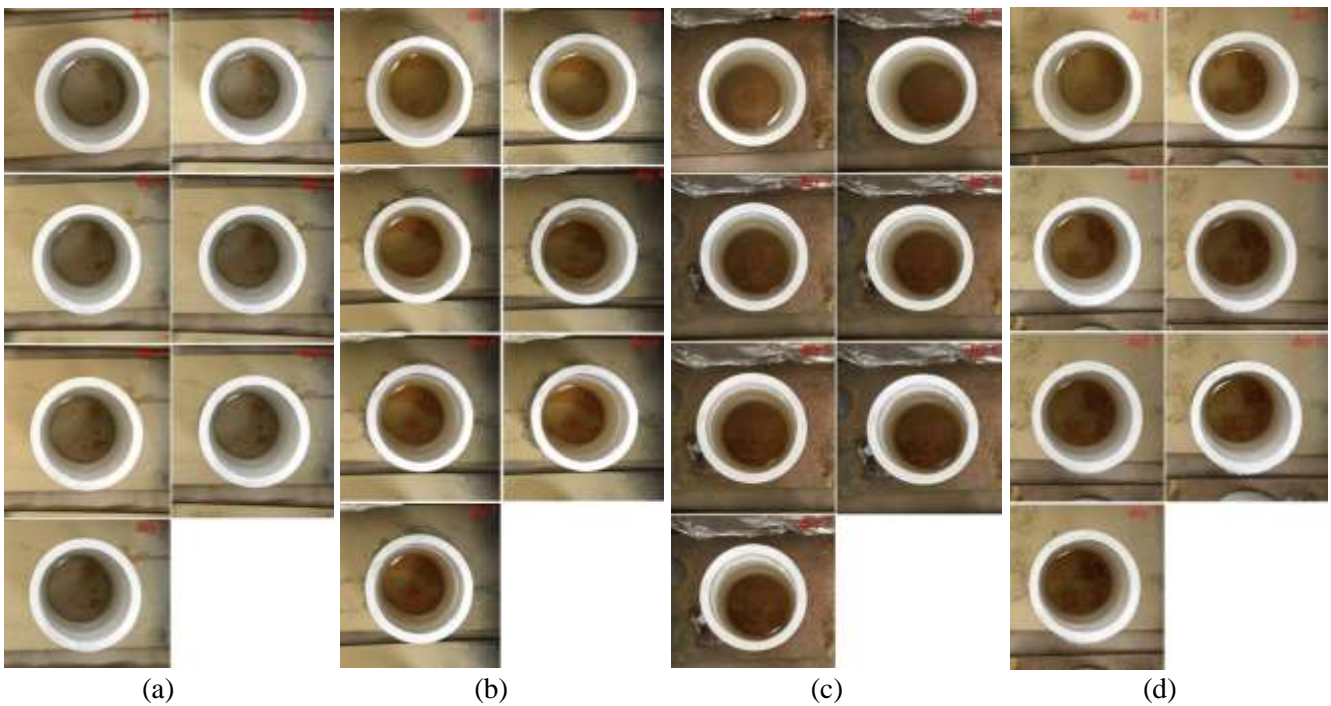


Figure 33 Corrosion test after seven days on (a) Sample #1, (b) Sample #2, (c) Sample #3, and (d) Sample #4.

Table 9 summarized the maximum wavelength changes monitored in 21 days period and Figure 34 shows the obtained center wavelength changes vs emerging time after eliminating the temperature effect for 21 days. From the graph, it can be seen that the curves from all the four samples have an approximately same trend, which is very encouraging for the development of the innovative sensing technology. Along with the corrosion happened, the strain was increasing coinstantaneous. A total changes of 60pm for Sample #2 and 30pm for Sample #1 and Sample #3 were noticed from the test results. After 15 days, consistently, all the samples were corroded into the coating as can be seen from the bottom right inset of Figure 34.

Table 9 Center wavelength changes for the four samples before and after the corrosion test (Sample #1~#4).

Sample Number	Wavelength Before Testing, nm	Wavelength After Adding 3.5% NaCl Solution, nm	Wavelength At End Point Of Data Collection (No Temperature Effect), nm	Maxmium Wavelength Changes After Solution Added (No Temperature Effect), nm
Sample 1	1555.98	1555.96	0.0189	0.0314
Sample 2	1551.94	1551.92	0.0496	0.06304
Sample 3	1551.89	1551.86	-0.0176	0.0192
Sample 4 Strain	1563.96	1563.95	0.0189	0.03186

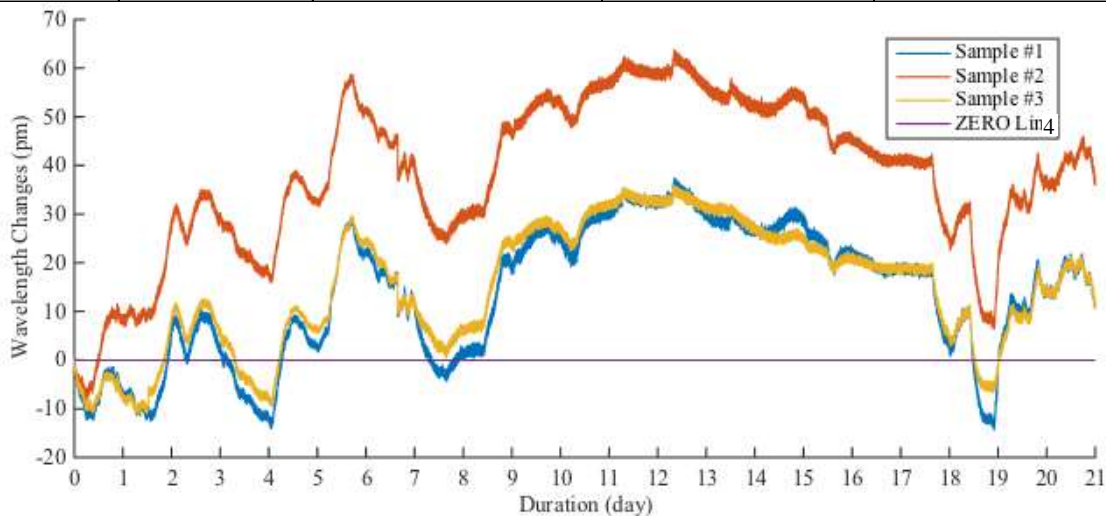


Figure 34 The variation of changes in the center wavelength of the embedded sensing system during 21 days in the NaCl solution (Sample #1~#4).

Figure 35 shows the monitored results for the embedded in-line FBG sensors on steel plates without coating (Sample #5 and #6) by emerging them in PVC tubes filled with 3.5% NaCl solution for 21 days. Being the same

as previous test, the wavelength changes of samples had been recorded continuously for entire test time with a sampling frequency of 10Hz. Table 10 shows the wavelength change at the end of experiment and the maximum wavelength change during test.

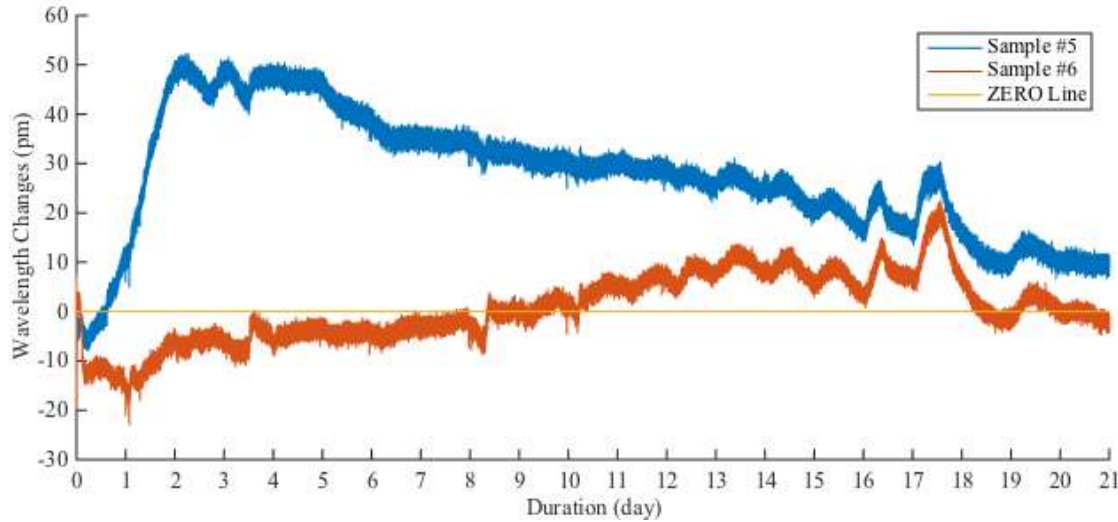


Figure 35 The variation of changes in the center wavelength of the embedded sensing system during 21 days in the NaCl solution (Sample #5,#6).

Table 10 Center wavelength changes for two samples during the corrosion test (Sample #5,#6).

Sample Number	Wavelength Before Test (nm)	Wavelength at the end of test (nm)	Maximum Wavelength change during test (nm)
Sample #5	1544.03	0.0123	0.0571
Sample #6	1531.95	-0.0012	0.0254

The visual inspection photos (Figure 33) were shown two different kinds of corrosion pattern – pin-point corrosion (Sample #1 and #5) and uniform corrosion (Sample #2, #4, and #6). In sensor reading data, two different types of curve were respectively reflecting two different types of corrosion pattern. In pin-point corrosion pattern, the strain reading curve in first 7 days has a steep positive slope. It's worth mentioning that the wavelength change curve of Sample #5, which is uncoated steel plate sample, has a steeper slope than the one of Sample #1, which is Cu-Al bronze coated steel plate sample. It took almost 9 days for Sample #1 to reach stable reading from sensor, and it only took 2 days for Sample #5 to reach a stable reading. This result shows that the coating could 4 ~ 5 times decrease pin-point corrosion expand. In uniform corrosion pattern, the sensor reading curve is relatively stable comparing to the ones of pin-point corrosion pattern. The curve gradually went up then after 13 ~ 15 days they began to drop. This result is because uniformly developed corrosion products brought less local effects comparing to pin-point corrosion pattern. In pin-point corrosion pattern, rapidly produced corrosion products do not have enough space to grow, resulting bring high local stress/strain. After more and more corrosion happened around the original pin-point corrosion, or over-grown corrosion products finally broke the original structure of its surroundings, the corrosion products had more and more space to release so that the stress/strain would gradually reduce.

5.4 Summary

In this section, ten plate samples were prepared and tested for accelerated corrosion tests by three graduate students, Xiao Liang, S. A. Galedari, and Fodan Deng, and one postdoc, Dr. M. SalimiJazi. The tested samples included four samples with embedded sensors and thermal sprayed Cu-Al Bronze coating (Sample 1~4), two samples without thermal coating but with embedded sensors (Sample 5~6), two reference samples with thermal sprayed coating but without embedded sensors (Sample 7~8), and two samples without any thermal sprayed coating (Sample 9~10). The test results from the accelerated corrosion tests showed that the embedded FBG sensing system not only can identify the initialization of the corrosion occurrence qualitatively, but also can identify corrosion type at the sensor locations, indicating the feasibility and effectiveness of the embedded FBG sensing system for steel corrosion assessment.

6 Corrosion Experiments and Results on Steel Pipes

To further investigate the effectiveness of the developed self-sensing thermal sprayed Cu-Al Bronze coating for steel pipe simultaneous corrosion mitigation and assessment, in this section, accelerated corrosion tests were performed on three pipe samples, including one steel pipe without thermal spraying coating with embedded sensing system and two steel pipes with coating and embedded sensing systems.

6.1 Sample Preparation

6.1.1 Pre-Spray Preparation Process

A new rotating fixture was designed by two undergraduate students, A. Perrault; C. M. Ferreira, and one graduate student, Babak Jahani, to hold pipe samples in front of spraying nozzle for coating deposition. Figure 36 shows the spraying set-up for spraying process. It includes several parts: an adjustable pipe fixing holder, a rotational axle connected to a speed-control instrument, and a manually movable spraying gun holder. Pipes with inner diameter from 1 inches to 12 inches can be placed on the holder for spraying. The pipe can rotate at various speeds which is adjustable from low to high speed during the spraying process to meet the requirement for different spraying thickness. The spraying gun holder is designed to move horizontally at constant speed to provide a uniform deposition on the surface of the pipe samples.



Figure 36 Spraying set-up for HVOF spraying of pipe samples.

Two pipe samples were prepared for HVOF deposition by the Ph. D. student, Fodan Deng. Each steel pipe sample had an outer diameter of 2.5 inches, a thickness of 0.203 inch, and a length of 4 inches as shown in Figure 37. Similar sensor embedment technique as used for steel plates in previous reports was applied to the steel pipe samples. One groove with 0.0625-inch width and approximately 0.0625-inch depth was made on each steel pipe sample in order to embed an OS1100 FBG strain sensor, which is also shown in the Figure 37.



Figure 37 Steel Pipe Sample

Two types of hypodermic tubes were used to protect FBG strain sensor and the communication fiber from damage during the HVOF spraying process. The hypodermic tube with an inner diameter of 0.01225 inch as shown in Figure 38(a), was used to protect the FBG sensing unit. M-Bond 200 epoxy was used to attach the sensing unit to the hypodermic tube as shown in Figure 38(b). The other type of hypodermic tube had an inner diameter of 0.028 inch, which was used for protecting communication fiber of the sensor, as shown in Figure 38(c). In order to provide a comprehensive protection for FBG strain sensors, an overlap of quarter inch length was made in each embedment, as shown in Figure 38(d). Overlap section of two types of tubes were attached to each other with M-Bond 200 epoxy as adhesive to make sure that there has no sliding between two types of tube.

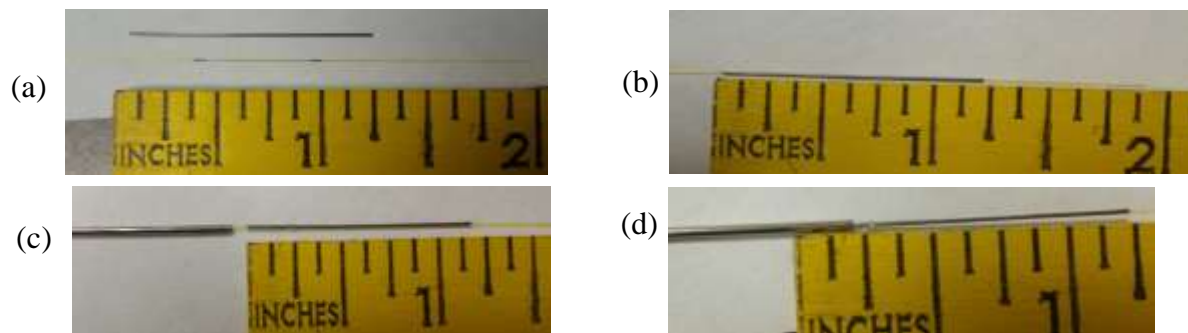


Figure 38 FBG Sensor Protection Process, (a) 0.01225 inch Hypodermic Tube, (b) FBG Strain Sensor with Protection, (c) Fiber Optic with Protect, and (d) Overlap of Two Types of Hypodermic Tubes.

The packaged fiber optic FBG sensor then was embedded inside the pre-fabricated groove on the surface of the pipe samples as shown in Figure 39(a). As mentioned in steel plate sample preparation section above, the metallic-stainless steel based adhesive (Durabond 954) was applied to attach the packaged sensor on the pipe surface. A 24-hour curing period was applied for the Durabond 954 adhesive before sandblasting, as shown in Figure 39(b).



Figure 39 Steel Pipe Sample Preparation, (a) Sensor Embedment on Steel Pipe and (b) Steel Pipe Samples with Durabond 954 Adhesive.

6.1.2 Thermal Spray Coating for Steel Pipe Samples

The prepared pipe samples were then coated by the Ph.D. student, S. A. Galedari, and Fodan Deng, and the postdoc, Dr. M. SalimiJazi. Figure 40 shows the spraying operation in this study. The prepared steel pipe samples with embedded sensors were sandblasted prior to the spraying as shown in Figure 41(a) following the ASTM standard. The sandblasted pipe samples were then sprayed using HVOF system and copper coating was deposited

uniformly on the surface of the pipes. It is worth mentioning that copper was selected as optimum coating. Figure 41(b) shows the pipe after spraying copper coating.



Figure 40 HVOF thermal spraying process for pipe samples.



(a)



(b)

Figure 41 Steel Pipe Sample (a) after Sandblasting and (b) after Coating deposition.

6.2 Accelerated Corrosion Tests and Results

Accelerated corrosion tests for steel pipe samples were performed by the Ph. D. student, Fodan Deng, through emerging samples to emerging them in PVC tubes filled with 3.5% NaCl solution for 21 days. The test set-up is shown in Figure 42. The wavelength changes of four samples had been recorded continuously for entire test time with a sampling frequency of 10Hz (shown in). After 15 days of monitoring, the wavelength change of Sample #2 suddenly reached 2,000 pm and it was exceeded the range of monitor instrument so that the curve for Steel Pipe Sample #2 was cut off around on the day 15. The wavelength change at the end of experiment and the maximum wavelength change during test are shown in Figure 43 and values are listed in the Table 11.



(a)



(b)

Figure 42 Test Set-Up Of Accelerated Corrosion Test For Steel Pipe Samples.

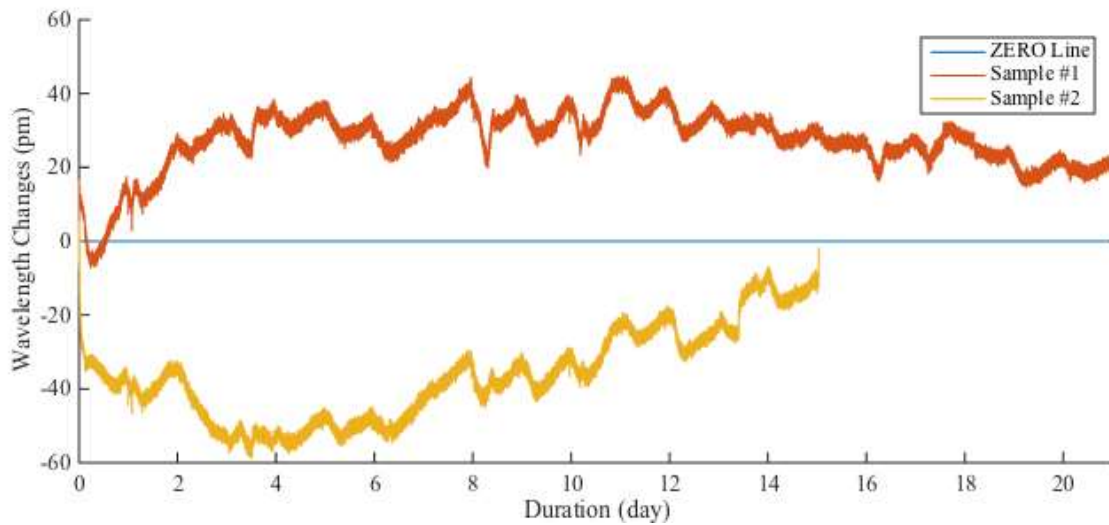


Figure 43 The variation in the center wavelength of the embedded sensing system during 21 days in the NaCl solution (Steel Pipe Sample #1,#2).

Table 11 Center wavelength changes for the steel pipe samples during the corrosion test

Sample Number	Wavelength Before Test (nm)	Wavelength at the end of test (nm)	Maximum Wavelength change during test (nm)
Sample #1	1543.87	0.0181	0.0493
Sample #2	1525.10	0.0063	0.0254

Similar to the steel plate samples, the corrosion developed on the steel pipe samples were also able to be classified into the same two categories – pin-point corrosion (Sample #2) and uniform corrosion (Sample #1). However, instead of getting positive slope in pin-point corrosion pattern in first one week, the sensor reading curve of Sample #2 were showing a negative slope. This result might be brought by the vertical placing of sensors. With the weight of corrosion products, the FBG sensors were under pressure more than under tension. After about one week, with more and more pin-point corrosion happened or overgrowth of corrosion products leading to broken original structure, the stress/strain level began to lower.

6.3 Summary

In this section, steel pipe samples with embedded sensors were coated by a combined efforts with two undergraduate students (A. Perrault and C. M. Ferreira), three graduate students (S. A. Galedari, Babak Jahani, and Xiao Liang), and one post doc (M. SalimiJazi). The accelerated corrosion tests were performed and analyzed by the Ph. D. student (F. Deng), on uncoated and coated steel pipe samples with embedded FBG sensing system in order to better understand the relationship between sensor reading and corrosion development. Experimental results showed promising achievements for the embedded sensing system to qualitatively detect corrosion and also distinguish two different types of corrosion pattern, indicating a potential effective corrosion assessment tool for pipeline industry.

7 Conclusion

In this project, a self-sensing thermal spraying mettalic coating was developed for pipeline application. The concept was proved and the new developed protective system approved to be effective to mitigate and assess corrosion for steel pipelines. There are two undergrate research assitants, two master students, two Ph. D. students, and one post doc worked on this project. The associated students gained valuable experiences through this project with rewarded intership and full-time job opportunities in related engineering fields. The detail technical conclusions can be drawn from this study as follows:

- 1) The Copper and Cu-Al Brone alloy coating using HVOF thermal spraying technique are very promising as for steel corrosion prevention and a thin layer of Cu-Al Brone alloy coating could significantly improve the corrosion resistance.
- 2) The developed LPFG based surface sensor is an effective approach to monitor corrosive environments on top of a steel pipe;
- 3) The embedment of a FBG sensor into a thermal spraying coating is challenging and the use of a layer of stainless-steel-based adhesive on top of the steel tube packaged FBG sensor can meet the challenge to embed the FBG sensors inside the coating;
- 4) The FBG embedded thermal spraying coating can monitor the corrosion for both steel plates and steel pipes qualitatively in real time and also indentify corrosion pattern;

The integrated sensing system enables the thermal sprayed metallic coating to be self-sensing when the coating is performing for corrosion prevention. It is an effective approach for simultaneous corrosion mitigation and assessment, which can be applied for pipelines. Future studies will be performed on the further improvement the corrosion mitigation of the coating using various sealing techniques and the further investigation of using the sensing system to quantitatively assess the corrosion, which is funded by the U.S. DOT PHMSA in 2015. More importantly, more students will get a chance to be involved in this innovative technology development in pipeline related engineering fields.

Publications based on This Study:

1. Y. Huang, "Fiber Optic Sensing System for In-Situ Simultaneous Monitoring of Water Stage, Quality and Temperature," Proc. of SPIE, (2014).
2. Y. Huang, L. Xiao, and F. Azarmi, "Innovative Fiber Optic Sensors for Pipeline Corrosion Monitoring," 2014 ASCE Pipelines conference, (2014).
3. Y. Huang, F. Tang, X. Liang, G. Chen, H. Xiao, and F. Azarmi, "Steel bar corrosion monitoring with long-period fiber grating sensors coated with nano iron/silica particles and polyurethane", Structural Health Monitoring, Vol. 14 (2), pp. 178-189, (2015).
4. Y. Huang, M. S. Jazi, and F. Azarmi, "Composite Coatings for Fibre Bragg Grating Sensor in High Temperature Environments", International Journal of Sensors and Sensor Networks, 3(2), pp. 12-17, (2015).
5. S. Abualigaedari, M. S. Jazi, F. Azarmi, Y. Huang, and X. Tongping, "Microstructural Properties of Air Plasma Sprayed Coating Consisting of Tungsten Carbide and Yttria Stabilized Zirconia", International Journal of Applied Ceramic Technology, Accepted (2015). S. A. Galedari, M. S. Jazi, F. Azarmi, A. Tangpong, and Y. Huang, "An Investigation on Microstructural Properties of Plasma Sprayed Tungsten Carbide Enhanced with Partially Stabilized Zirconia," 2015 International Thermal Spray Conference and Exposition, (2015).
6. X. Liang, Y. Huang, S. A. Galedari, and F. Azarmi, "Pipeline Corrosion Assessment Using Embedded Fiber Bragg Grating Sensors," 2015 SPIE conference of smart structures & NDE, March 24 2015, San Diego, CA. (Paper ID: 9435-69).
7. Y. Huang, X. Liang, S. A. Galedari, and F. Azarmi, "Integrated Fibre Optic Sensing System for Pipeline Corrosion Monitoring", 2015 ASCE pipelines conference, August 23-26 2015, Baltimore, Maryland. (Paper ID: 141).
8. F. Deng, Y. Huang, and F. Azarmi, "In-line Fiber Bragg Grating Sensors for Steel Corrosion Detection," 2016 SPIE conference of smart structures & NDE, March 24 2016, Las Vegas, NV

Students Involved in This Study:

- Undergraduate Research Assistants:
A. Perrault; C. M. Ferreira
- Graduate Research Assistants:

S. A. Galedari (Ph. D. student, in process); Fodan Deng (Ph. D. student, in process); Babak Jahani (Master student, in process), Xiao Liang (Master student, graduated).

- Post-Doc Research Associate:

Dr. M. SalimiJazi

References

1. Pipeline corrosion, Michael Baker Jr., U.S. Department of Transportation, Inc. November 2008.
2. Corrosion and corrosion control of iron pipeline, Richard W. Bonds, et al., American water work association, 2005.
3. Corrosion Costs and Prevention Strategies in the United States, Koch, G.H., et al., Federal Highway Administration, FHWA-RD-01-156. Washington, DC. (March 2002).
4. Corrosion Handbook, R. Winston Revie, Herbert Henry Uhlig.
5. Control of pipeline corrosion, A. W. Peabody, 2nd edition, p, 280.
6. R. Baboian, NACE Corrosion Engineer's Reference Book, Third Edition, Published by NACE International, Houston, TX, USA, 2002
7. NACE Standard, Control of External Corrosion on Underground or Submerged Metallic Piping Systems, NACE Standard No. SPO169, 2007
8. M. Manivannan, S. Rajendran, and SA. S. Prabha, "Inhibitors for Prevention of Corrosion of Metals in Sea Water: An Review," Eur. Chem. Bull., Vol. 1, No. 8, pp. 317-329, 2012
9. ASM International, Metals Handbook, Second Edition, Published by ASM International, Materials Park, Ohio, USA, 1998
10. AWWA C203-97 and Addendum C203a-99, Coal-Tar Protective Coating and Linings for Steel Water Pipelines – Enamel and Tape – Hot Applied, AWWA, Denver, CO., 1997/99
11. S. W. Guan, "100% Solid Rigid Polyurethane Coatings Technology and Its Application on Pipeline Corrosion Protection," ASCE Journal of Pipelines, pp.156-165, 2003
12. G. Munger and L. D. Vincent, Corrosion Prevention by Protective Coatings, Second Edition, NACE Publication, 1999
13. AWWA C213-96, Fusion-Bonded Epoxy Coating for the Interior and Exterior of Steel Water Pipeline, AWWA, Denver, CO., 1996
14. AWWA C222-99, Polyurethane Coatings for the Interior and Exterior of Steel Pipelines and Fittings, AWWA, Denver, CO., 1999
15. S. Kuroda and J. Kawakita, "Marine Exposure Tests of Thermal Sprayed Coatings in Japan," Thermal Spray 2003: Advancing the Science & Applying the Technology, (Ed.) C. Moreau and B. Marple, Published by ASM International, Materials Park, Ohio, USA, pp. 343- 352, 2003
16. F. J. Antunes, V. R. S. Sá Brito, I. N. Bastos, and H. R. M. Costa, "Characterization of FeCr and FeCoCr Alloy Coatings of Carbon Steels for Marine Environment Applications," Applied Adhesion Science, Vo. 1, No. 3, pp.1-10, 2013
17. T. Bernecki, Surface science, J.R. Davis (Ed.), Handbook of Thermal Spray Technology, ASM International, Materials Park, OH, pp. 14-35, 2004
18. R. Arrabal, A. Pardo, M. C. Merino, M. Mohedano, P. Casajus, and S. Merino, "Al/SiC Thermal Spray Coatings for Corrosion Protection of Mg–Al Alloys in Humid and Saline Environments," Surface Coating Technology, Vol. 204, pp. 2767-2774, 2010
19. P. K. Aw, A. L. K. Tan, T. P. Tan, and J. Qiu, "Corrosion Resistance of Tungsten Carbide Based Cermet Coatings Deposited by High Velocity Oxy-Fuel Spray Process," Thin Solid Films, Vo. 516, pp.5710-5715, 2008
20. J. C. Tan, L. Looney, and M. S. J. Hashmi, "Component Repair Using HVOF Thermal Spraying," Journal of Material Process Technology, Vo. 92-93, pp. 203-208, 1999
21. J. Brodar, "Zinc Metallizing Protects Dam after 20 Years," Journal of Protective Coatings and Linings, pp. 49-55.D, 1995
22. Tordonato, Laboratory Evaluation of Metalized Coatings for Use on Reclamation Infrastructure, Bureau of Reclamation, Technical Service Center, Denver, Colorado, Technical Memorandum No. MERL-2012-1, May 2012
23. CSA, Sprayed Metal Coatings for Atmospheric Corrosion Protection, G189-1966, Toronto, Ontario, Canada: Canadian Standards Association, 1966, Reaffirmed in 1980

24. J. Ellor, W. Young, and J. Repp, NCHRP Report 528: Thermally Sprayed Metal Coatings to Protect Steel Pilings, National Cooperative Highway Research Program, Transportation Research Board, 2004
25. ASTM G96-90, Standard Guide for Online Monitoring of Corrosion in Plant Equipment (Electrical and Electrochemical Methods), ASTM International (West Conshohocken: PA), 2008
26. F. Mansfeld, Electrochemical Methods of Corrosion Testing ASM handbook, (ASM International:OH), 2003
27. ASM Handbook, Vol 13, (originally published as Metals Handbook, Vol 13, 9th ed.), ASM international, 1987
28. K. S. Rajagopalan et al., Corrosion, No. 15, 1959, p 631.
29. V. T. Rathod, M. D. Roy, and S. Gopalakrishnan, "Lamb Wave Based Identification and Parameter Estimation of Corrosion in Metallic Plate Structure Using a Circular PWAS Array," Proceeding of the 16th SPIE Annual Symposium on Smart Structures and Materials, Vol. 7295, 2006
30. D. G. Steven, "Sensor Technology Innovation for the Advancement of Structural Health Monitoring: a Strategic Program of US-China Research for the Next Decade," Smart Structures and Systems, Vol. 3, pp. 221-244, 2007
31. G. Qiao, Z. Zhou, and J. Ou, "Thin Fe-C Alloy Solid Film Based Fiber Optic Corrosion Sensor," Proceedings of the 1st IEEE Conference on Nano/Micro Engineered and Molecular Systems, pp. 541-544, 2006
32. C. K. Y. Leung, K. T. Wan, and L. Chen, "Novel Optical Fiber Sensor for Steel Corrosion in Concrete Structures," Sensors, Vol. 8, pp. 1960-1976, 2008
33. S. A. Wade, C. D. Wallbrink, G. McAdam, S. Galea, B. R. W. Hinton, and R. Jones, "A Fiber Optic Corrosion Fuse Sensor Using Stressed Metal-coated Optical Fibers," Sensors and Actuators B: Chemical, Vol. 131, pp. 602-608, 2008
34. G. Qiao and J. Ou, "Corrosion Monitoring of Reinforcing Steel in Cement Mortar by EIS and ENA," Electrochemical Acta., Vol. 52, pp. 8008-8019, 2007
35. N. P. Dickerson and S. L. Wood, "Wireless Low-cost Corrosion Sensors for Reinforced Concrete Structure," Proceedings of the 12th SPIE Annual Symposium on Smart Structures and Materials, Vol.5765, pp. 493-503,2005
36. V. S. Agarwala and S. Ahmad, "Corrosion Detection and Monitoring – A Review," Proc. of NACE International 2000, Paper No.271, 2000
37. S. Abderrahmane, A. Himour, R. Kherrat, E. Chailleux, N. Jaffrezic-Renault, and G. Stremmsdoerfer, "An Optical Fiber Corrosion Sensor with an Electroless Deposit of Ni-P," Sensors and Actuators B: Chemical, Vol. 75, pp. 1-4, 2001
38. M. Benounis and N. Jaffrezic-Renault, "Elaboration of an Optical Fiber Corrosion Sensor for Aircraft Applications," Sensors and Actuators B: Chemical, Vol. 100 , pp.1-8, 2004
39. Z. Zheng, X. Sun, and Y. Lei, "Monitoring Corrosion of Reinforcement in Concrete Structures via Fiber Bragg Grating Sensors," Front. Mech. Eng. of China, Vol. 4, No. 3, pp. 316-319, 2009
40. S. Dong, G. Peng, and Y. Luo, "Preparation Techniques of Metal Clad Fibers for Corrosion Monitoring of Steel Materials," Smart Mater. Struct., Vol. 16, pp. 733-738, 2007
41. W. Hua, H. Cai, M. Yang, X. Tong, C. Zhou, and W. Chen, "Fe-C-coated Fibre Bragg Grating Sensor for Steel Corrosion Monitoring," Corrosion Science, Vol. 53, pp. 1933-1938, 2010
42. K. R. Cooper and L. Innovations, "Optical Fiber-Based Corrosion Sensor Systems for Health Monitoring of Aging Aircraft," Proceeding of IEEE, Vol. 128, pp. 540-552-5, 2001
43. G. Kear a, B.D. Barker, F.C. Walsh, "Electrochemical corrosion of unalloyed copper in chloride media, a critical review", Corrosion Science, Vol.46, pp.109-135, 2004
44. N. K. Allam, A. A. Nazeer, G. I. Youssef, and E. A. Ashour, "Electrochemical and stress corrosion cracking behavior of α -Aluminum Bronze and α -Brass in nitrite solutions: a comparative study", Corrosion, Vol. 69, No. 1, pp. 77-84, 2013.
45. J. E. Tibballs and R. Erimescub, "Corrosion of dental aluminium bronze in neutral saline and saline lactic acid", Dental Materials, Vol. 22, pp.793-798, 2006.
46. Y. Huang, F. Tang, X. Liang, G. Chen, H. Xiao, and F. Azarmi, "Steel bar corrosion monitoring with long period fiber grating sensors coated with nano iron/silica particles and polyurethane", Structural Health Monitoring, November 24, 2014 1475921714560070, 2014.
47. Y. Huang, Z. Gao, Z. Zhou, G. Chen, and H. Xiao, "Long period fiber grating sensors coated with nano iron/silica particles for corrosion monitoring", Smart Materials and Structure, Vol. 22, No. 7, pp. 075018, 2013.